이학박사 학위논문

알츠하이머병에서 타우 단백질의 수용체 매개 전파와 기억 손실에 관한 연구

A study on the receptor-mediated tau transmission and memory loss in Alzheimer's disease

2023년 2월

서울대학교 대학원

협동과정 뇌과학전공

김 유 빈

알츠하이머병에서 타우 단백질의 수용체 매개 전파와 기억 손실에 관한 연구

A study on the receptor-mediated tau transmission and memory loss in Alzheimer's disease

지도 교수 정 용 근

이 논문을 이학박사 학위논문으로 제출함

2023년 1월

서울대학교 대학원

협동과정 뇌과학전공

김 유 빈

김유빈의 이학박사 학위논문을 인준함

2023년 1월

위 원 장 _____ (인)

부위원장 _____ (인)

위 원 _____ (인)

위 원 _____ (인)

위 원 _____ (인)

A study on the receptor-mediated tau transmission and memory loss in Alzheimer's disease

Advisor: Professor Yong-Keun Jung, Ph.D.

Submitting a Ph.D. Dissertation of
Biological Sciences

January, 2023

Graduate School of Natural Sciences
Seoul National University
Brain Science Major

Youbin Kim

Confirming the Ph.D. Dissertation written by
Youbin Kim
January, 2023

Chair _____(Seal)

Vice Chair _____(Seal)

Examiner _____(Seal)

Examiner _____(Seal)

Examiner _____(Seal)

Abstract

A study on the receptor-mediated tau transmission and memory loss in Alzheimer's disease

Youbin Kim
Interdisciplinary Program in Brain Science
Graduate School of Natural Sciences
Seoul National University

In tauopathies, brain regions with tau accumulation strongly correlate with clinical symptoms and spreading of misfolded tau along neural network leads to disease progression. Accumulating evidence suggests that glial cells contribute to the process of tau propagation. However, the underlying mechanisms by which tau proteins enter neurons during pathologic propagation remain unclear.

To identify membrane receptors responsible for neuronal propagation of tau oligomers, I established a cell-based tau uptake assay and screened cDNA expression library. From a genome-wide cell-based functional screening, RAGE (receptor for advanced glycation end products) was isolated to stimulate the cellular uptake of tau oligomers. *Rage* deficiency

reduced neuronal uptake of pathological tau prepared from rTg4510 mouse brains or cerebrospinal fluids from Alzheimer's disease patients, and slowed tau propagation between neurons cultured in a three-chamber microfluidic device. RAGE levels were increased in the brains of rTg4510 mice and tau oligomer-treated neurons. *Rage* knockout ameliorated memory loss after injection with GFP-P301L tau AAV. Treatment of RAGE antagonist FPS-ZM1 alleviated cognitive impairment in rTg4510 mice by blocking transsynaptic tau propagation and inflammatory responses.

Also, I explored the role of immunoreceptor TauIR (tau immunoreceptor) in neuronal propagation of tau oligomers. In microglia, tau oligomers induced TauIR activation which in turn increased cellular tau uptake. *TauIR* deficiency or blocking TauIR using anti-TauIR antibody reduced tau uptake into microglia. Tau-induced TauIR activation increased pro-inflammatory cytokines. In neurons, *TauIR* deficiency or anti-TauIR antibody treatment also reduced cellular tau uptake. *TauIR* knockout ameliorated cognitive impairment in rTg4510 mice.

These results suggest that RAGE and TauIR on neurons and microglia bind to pathological tau, and facilitate neuronal tau propagation and microglial inflammatory responses. Therefore, blocking the function of two membrane receptors RAGE and TauIR may suppress the progression of tau pathology and development of memory loss in tauopathies.

Keywords : Tau propagation, Tau oligomer, Neuroinflammation, RAGE, Tau immunoreceptor, FPS-ZM1

Student Number : 2015-20501

Table of Contents

List of Figures

Chapter 1. Introduction

Tau pathophysiology in Alzheimer's disease

Microtubule-associated protein tau is neuronal protein which was found to be associated to microtubules (Weingarten et al., 1975). Tau protein has intrinsically disordered structure but contains three or four carboxy-terminal repeat domains depending on the isoform that mediate binding to microtubules (Lee et al., 1988; Amos, 2004). In physiological conditions, tau mainly localizes in the neuronal axons and regulates the dynamics of microtubules through its repeat domains, therefore provides structural support for neurons (Biswas & Kalil, 2018; Caceres & Kosik, 1990; Dawson et al., 2001). In pathological conditions, however, post-translational modifications or truncations of tau protein result in detachment of tau from microtubules, misfolding and aggregation via tau repeat domains (Alquezar et al., 2021).

Tau inclusions inside the neurons are the pathological hallmark of tauopathies including Alzheimer's disease (AD) (Spillantini & Goedert, 2013). In contrast to the unstructured nature of tau, misfolded tau proteins become prone to aggregate into oligomers, paired helical filaments and neurofibrillary tangles (Kidd, 1963; Stelzmann et al., 1995). In this process, tau species that function as a pathological seed enable the rapid aggregation of tau, and thus play an important role in the development of tau pathology (Knowles et al., 2014; Mirbaha et al., 2018).

Neuronal tau transmission in Alzheimer's disease

It has long been recognized that the distribution of tau inclusion widens during disease progression and strongly correlates with clinical stage in AD (Braak & Braak, 1991). Recent advances in tau imaging enabled the prediction of patient-specific patterns of tau spreading along neural connectivity (Brown et al., 2019; Vogel et al., 2021). Previous studies have focused on demonstrating transsynaptic propagation of various tau species *in vitro* (Wu et al., 2013; Takeda et al., 2015) and *in vivo* (Clavaguera et al., 2009; de Calignon et al., 2012; Wegmann et al., 2015; Guo et al., 2016). It has placed emphasis on macropinocytosis-mediated tau internalization in neurons (Frost et al., 2009; Wu et al., 2013), mediated in large part by heparin sulfate proteoglycans (HSPGs), which bind to extracellular tau aggregates and promote their cellular uptake (Holmes et al., 2013). Low-density lipoprotein receptor-related protein 1 (LRP1) operates cooperatively with HSPGs to control tau entry into neurons (Rauch et al., 2020), while its contribution to tau pathogenesis has not been determined.

In addition, dynamin-dependent endocytosis pathway was proposed to selectively regulate internalization of P301S tau aggregates into human iPSC-derived neurons (Evans et al., 2018). BIN1/Amphiphysin2, the genetic risk factor for late-onset AD, was also shown to modulate clathrin-mediated endocytosis of P301L tau aggregates and their transsynaptic propagation *in vitro* (Calafate et al., 2016). Given that tau strains found in various tauopathies are highly heterogeneous (Clavaguera et al., 2013; Kaufman et

al., 2016), there is an urgent need to identify the diverse modulators that are responsible for pathologic propagation of toxic tau forms. Although tau aggregates are considered to be the major pathological form to be transmitted between neurons, the precise mechanism by which they enter neurons largely remains unclear.

Microglial contribution to tau transmission

The activation of microglia and chronic neuroinflammation have been observed in the brains of AD (Kinney et al., 2018). Microglial activation in early AD pathogenesis may play a neuroprotective role through the clearance of pathogenic tau aggregates, however, chronic microglial activation in late AD pathogenesis may play a neurotoxic role through the inflammatory responses (Javanmehr et al., 2022; Paolicelli et al., 2022). For example, previous report demonstrated that microglial activation precedes tau pathology development in P301S tau transgenic mouse (Yoshiyama et al., 2007). Sustained Interleukin-1β production also exacerbated tau pathology in 3xTg-AD mouse model for AD (Ghosh et al., 2013).

Microglia express diverse activating and inhibitory immunoreceptors that modulate their functions (Wang & Colonna, 2019). Interestingly, the major activating immunoreceptor triggering receptor expressed on myeloid cells 2 (TREM2), and inhibitory immunoreceptor paired immunoglobulin-like type 2 receptor α (PILRα) and CD33 were identified through genome-wide association studies (GWAS) as a risk factor of developing late-onset AD

(Jonsson et al., 2013; Lambert et al., 2013; Rathore et al., 2018). In addition, TauIR (tau immunoreceptor) has been reported to be upregulated in the brains of P301L tau transgenic mice and human AD patients (Bonham et al., 2018; Momtazmanesh et al., 2020). However, its contribution to tau pathogenesis has not been determined.

In the present study, I performed cell-based assays to isolate membrane receptors responsible for cellular uptake of tau oligomers. I identified a receptor for advanced glycation end products (RAGE, also called AGER) from the screen, and found that RAGE mediates neuronal uptake and transmission of pathological forms of tau. Moreover, RAGE was required for tau-induced memory loss and blocking the interaction between RAGE and tau oligomers ameliorated cognitive impairment in rTg4510 mice.

In addition, I examined the role of TauIR in tau spread and pathogenesis. In microglia, TauIR is activated by tau oligomers, increasing tau uptake and inflammatory responses. Interestingly, anti-TauIR monoclonal antibody treatment significantly blocked TauIR function in microglia. In neurons, *TauIR* deficiency or anti-TauIR antibody treatment also reduced cellular tau uptake. *TauIR* knockout ameliorated cognitive impairment in rTg4510 mice. Thus, I have identified two membrane receptors RAGE and TauIR which play an important role in tau pathogenesis and memory loss in AD.

Chapter 2. RAGE Transmits Tau Pathology and Behavioral Deficits in Alzheimer's Disease

2.1. Results

Isolation of RAGE as a prominent receptor for tau oligomer uptake

To identify membrane receptors responsible for neuronal propagation of tau oligomers, I established a cell-based tau uptake assay. Purified His-tagged human tau protein was labeled with DyLight 488 (DyLight 488-tau) and was allowed to form aggregates after incubation with heparin. Using fast protein liquid chromatography (FPLC), I found that tau aggregates occurred mostly as oligomeric (10-20 units) and fibrillar (≥ 40 units) forms (Figure 2.1.A and C).

I have collected mammalian expression complementary DNAs (cDNAs) encoding full-length human and mouse transmembrane proteins (total 1,523). For the assay, SH-SY5Y human neuroblastoma cells were transfected with each cDNA and incubated with DyLight 488-tau aggregates (Figure 2.2.A). From the screen, RAGE most efficiently mediated internalization of tau aggregates by the transfected cells (Figure 2.2.B and C). In the assay, overexpression of RAGE or recently reported tau receptor LRP1 (Rauch et al., 2020) did not affect the basal level of the other in SH-SY5Y cells (Figure 2.2.D-F). Monomeric, oligomeric and fibrillar forms of biotin-labeled tau proteins (biotin-tau) were then prepared and assayed for their interaction with RAGE. The results revealed that RAGE bound to a

broad array of tau forms, but with significant preference for tau oligomers (Figure 2.3.A and B). When assessed the lysosomal activity using DQ-red-BSA, treatment of tau oligomers reduced lysosomal activity in a dose-dependent manner (Figure 2.4.A and B). Overexpression of RAGE increased lysosomal activity in a low concentrations of tau oligomers, which also reduced in a dose-dependent manner to a level comparable to control (Figure 2.4.A and B). Therefore, the increased tau accumulation in RAGE-expressing cells is not the result of reduced tau degradation.

Previous studies have demonstrated that tau oligomers derived from brains of rTg4510 mouse and human AD patients appear as low-molecular-weight (LMW) forms (~150-195 kDa) and high-molecular-weight (HMW) forms (~669-1300 kDa) (Lasagna-Reeves et al., 2012; Wu et al., 2013; Takeda et al., 2015). Similarly, I could further divide tau oligomer species into LMW (2-4 units) and HMW (10-20 units) forms using FPLC (Figure 2.1.B and C). Incubating primary cultured wild-type (WT) and *Rage* knockout (KO) neurons with tau oligomers revealed that cellular uptake of LMW and HMW tau oligomers by *Rage* KO neurons significantly diminished as compared to WT neurons (Figure 2.5.A and B). Interestingly, the levels of LRP1 were a little increased in *Rage* KO neurons compared to WT neurons (Figure 2.5.C and D). Thus, the decrease of tau uptake by *Rage* KO is LRP1-independent. I then prepared biotin-tau oligomers, assayed for their interaction with RAGE by treating WT and *Rage* KO neurons, and subtracted tau binding to *Rage* KO neurons from tau binding to WT

neurons. The dissociation constants (K_d) for LMW and HMW tau oligomers binding to RAGE were 43.47 nM and 24.96 nM equivalent of tau monomer, respectively (Figure 2.5.E).

Rage knockout reduces pathologic tau uptake in neurons and microglia

Given that diverse tau strains are subject to neuronal propagation (Clavaguera et al., 2013; Kaufman et al., 2016), I assessed neuronal uptake of tau proteins prepared from rTg4510 mice, which express a human P301L mutant tau under the control of the Ca^{2+}-calmodulin kinase II (CaMKII) promoter (SantaCruz et al., 2005). When treated with the phosphate-buffered saline (PBS)-soluble brain extracts from rTg4510 mice which mainly contain LMW oligomers and rare (less than 10%) HMW tau oligomers (Takeda et al., 2015), human P301L tau proteins were observed inside the WT neurons, while it was significantly decreased in *Rage* KO neurons (Figure 2.6.A and B). I also tested uptake of the tau proteins from the cerebrospinal fluid of patients with AD (AD CSF) containing phospho-tau181 and T22-reactive tau oligomer (Schoonenboom et al., 2012; Gordon et al., 2016) (Figure 2.6.C). Similarly, neuronal uptake of tau proteins in AD CSF was active in WT neurons but was significantly impaired in *Rage* KO neurons (Figure 2.6.D and E). Moreover, *Rage* deficiency also blocked neuronal tau uptake *in vivo* when purified tau oligomers were injected into the hippocampus of WT and *Rage* KO mice (Figure 2.7.A-C).

Since RAGE is also expressed in microglia and astrocytes (Lue et al., 2001; Sasaki et al., 2001), I tested whether RAGE mediates tau uptake into these cells. I found that primary cultured WT microglia and astrocytes both readily internalized extracellular tau oligomers (Figure 2.8.A and B). In microglia, *Rage* KO reduced tau oligomer uptake as seen in neurons (Figure 2.8.A). However, uptake of tau oligomers into astrocytes was unaffected by *Rage* deficiency (Figure 2.8.B). Recent studies have shown that tau aggregates activate microglia, which promotes tau pathogenesis via releasing tau seeds and/or inflammatory cytokines (Asai et al., 2015; C. Wang et al., 2022). To examine whether RAGE-mediated tau uptake in microglia affects inflammatory responses, we generated *Rage* KO in BV2 mouse microglial cells (Figure 2.9.A). Similarly seen in primary cultured microglia, tau uptake was significantly reduced in *Rage* KO BV2 cells (BV2/sg*Rage*) compared to control BV2 cells (BV2/sgControl) (Figure 2.9.B). In cell conditioned medium, the levels of IL-1β were significantly increased by treatment with tau oligomers in BV2/sgControl cells, but this increase of IL-1β was reduced in BV2/sg*Rage* cells (Figure 2.9.C). These results indicate that RAGE plays a role in tau-mediated inflammatory responses in microglia.

Rage knockout reduces neuron-to-neuron tau propagation

To assess the role of RAGE in the transsynaptic tau propagation *in vitro*, I used a three-chamber microfluidic device that enabled observation of

neuron-to-neuron transfer via axon extension across the chambers (Park et al., 2006; Wu et al., 2013; Takeda et al., 2015; Calafate et al., 2016). For this assay, primary hippocampal neurons were cultured in the three chambers: WT neurons in the 1st chambers (C1), and WT or *Rage* KO neurons in the 2nd and 3rd chambers (C2 and C3) (Figure 2.10.A). I applied a volume difference of 50 μl between chambers (lesser volume on the C1) to maintain fluidic isolation between the chambers, used an adenovirus to overexpress GFP-fused human tau (GFP-tau) in C1 neurons, and evaluated GFP-tau propagation from C1 to C2 and C3 (Figure 2.10.A). Using dot blot assays, I confirmed robust formation of detergent-insoluble tau aggregates within neurons transduced with GFP-tau adenovirus compared to neurons treated with tau oligomers (Figure 2.10.B). After 14 days of adenoviral transduction, GFP-tau aggregates spread from the C1 to C3 neurons, and ~40% of C3 neurons were GFP-tau-positive in both WT and *Rage* KO neurons (Figure 2.10.C and D). When measured the amount of propagated GFP-tau, however, *Rage* deficiency reduced neuronal GFP-tau propagation by ~20% (Figure 2.10.C and D). These results imply that RAGE contributes to pathologic tau propagation.

RAGE V-C1 domains bind to tau oligomers to facilitate tau uptake

To characterize the interaction between RAGE and tau oligomers in detail, I generated several RAGE mutants lacking the extracellular V, C1, or C2 domain (Figure 2.11.A). Overexpressing RAGE mutants in SH-SY5Y cells

revealed that deletion of the V or C1 domain reduced cellular uptake of tau oligomers (Figure 2.11.B and C). Thus, RAGE V and C1 domains are necessary for the internalization of tau oligomers. Importantly, the G82S polymorphism of RAGE in its V domain (Figure 2.11.A) was reported to associate with the increased AD susceptibility (Li et al., 2009; Daborg et al., 2010) and to promote glycosylation of RAGE, which leads to structural change and enhances ligand binding (Hofmann et al., 2002; Osawa et al., 2007; Park et al., 2011). Notably, overexpressing G82S RAGE slightly increased tau binding (Figure 2.11.D and E), suggesting the effect of RAGE glycosylation on tau binding and uptake.

I then assessed the effect of RAGE antagonist FPS-ZM1 on tau uptake. FPS-ZM1 binds to the V domain and competitively inhibits the binding of RAGE ligands including $A\beta_{42}$ oligomers (Deane et al., 2012; Bongarzone et al., 2017) (Figure 2.12.A). Co-treatment with FPS-ZM1 inhibited uptake of tau oligomers into primary cultured neurons (Figure 2.12.A and B). Because RAGE is also known to interact with Aβ (Yan et al., 1996; Deane et al., 2003) through its V and C1 domains, I compared RAGE interaction with tau oligomers to $A\beta_{42}$ oligomers in SH-SY5Y cells. Synthetic $A\beta_{42}$ peptide was incubated at 4℃ for at least 24 h to form oligomers, which are mostly trimers and tetramers (Kam et al., 2013). When simultaneously treated RAGE-expressing SH-SY5Y cells with tau and $A\beta_{42}$ oligomers, I found that the presence of tau oligomers efficiently reduced cellular uptake of $A\beta_{42}$

oligomers (Figure 2.12.C), indicating that their binding to RAGE is competitive. Notably, co-treatment of tau oligomers or $A\beta_{42}$ oligomers with FPS-ZM1 blocked cellular uptake of tau oligomers as efficiently as $A\beta_{42}$ oligomers in a dose-dependent manner (Figure 2.12.D). Therefore, RAGE antagonist FPS-ZM1 blocks cellular uptake of tau oligomers as well as $A\beta_{42}$ oligomers.

Tau oligomers upregulate RAGE expression in neurons

To further investigate the role of RAGE in tau pathogenesis, I analyzed the pattern of RAGE expression in the brains of rTg4510 mice, which express a human P301L tau largely restricted to forebrain structures (SantaCruz et al., 2005). Remarkably, the hippocampal neurons of the rTg4510 mice showed increased RAGE expression compared to the neurons of the age-matched nontransgenic (NonTg) mice (Figure 2.13.A and B). Neurons with higher pathologic tau accumulation showed higher RAGE expression (Figure 2.13.B). Also, RAGE expression increased up to five-fold in the primary cultured neurons upon treatment with tau oligomers (Figure 2.14.A and B).

RAGE-ligand binding is known to activate MAPK/NF-κB pathway and lead to expression of RAGE itself (Kierdorf & Fritz, 2013). Treatment of tau oligomers also induced nuclear translocation of NF-κB p65 and increased RAGE expression (Figure 2.15.A and B), which was blocked by interfering RAGE-tau binding with FPS-ZM1 (Figure 2.15.C and D). Thus,

neuronal RAGE levels are upregulated by tau oligomers, which in turn likely enhances tau propagation in a vicious cycle.

RAGE blockade ameliorates behavioral abnormality

I then prepared an adeno-associated virus for the expression of GFP-tau with P301L mutation (GFP-P301L tau AAV) in the hippocampus and examined whether RAGE takes part in tau-induced behavioral deficits. I performed behavioral tests after 5 months of unilateral GFP-P301L tau AAV injection into the hippocampus CA3 region of WT and *Rage* KO mice (Figure 2.16.A). Interestingly, WT mice exhibited significant decline in spatial memory in the Y-maze test (Figure 2.16.B), learning and memory deficits in the novel object recognition test (Figure 2.16.C) and passive avoidance test (Figure 2.16.D). On the contrary, *Rage* KO mice did not develop such cognitive impairment (Figure 2.16.B-D). When examined for tau propagation, MC1-positive misfolded tau was found in the GFP-positive CA3 neurons in the injection area of WT mice and was also found in the GFP-negative CA1 neurons, showing transsynaptic tau propagation in the hippocampus (Figure 2.16.E). However, MC1-positive misfolded tau was not found in the CA1 neurons of *Rage* KO mice (Figure 2.16.E).

To assess whether neuronal RAGE is crucial for tau propagation, I again injected GFP-P301L tau AAV into the hippocampus CA3 region of WT and *Rage* KO mice, and then expressed full-length (FL) or tau-binding defective ΔV mutant RAGE in the neurons of *Rage* KO mice by injection of AAV

expressing RAGE FL or ΔV under CaMKIIa promoter into the cerebral ventricle (Figure 2.17.A and B). After 8 weeks of GFP-P301L tau AAV injection, CP13-positive pathological tau was found in the GFP-positive CA3 neurons in the injection area of both WT and *Rage* KO mice (Figure 2.17.C). The GFP-positive or CP13 pathological tau-positive neurons were found in the CA2 neurons of WT mice, showing transsynaptic tau propagation in the hippocampus (Figure 2.17.C). Neuronal reconstitution of *Rage* KO mice with RAGE FL AAV rebuilt the active tau propagation comparable to WT mice, but *Rage* KO mice reconstituted with RAGE ΔV AAV did not show such tau propagation (Figure 2.17.C). These results indicate that the binding of tau and RAGE in neurons is essential in *in vivo* tau propagation.

By assessing cognitive functions in rTg4510 mice, I further tested whether blocking the RAGE-tau interaction using RAGE antagonist could delay tau pathogenesis. The rTg4510 mice exhibit tau pretangles within their cortex as early as 2.5 months of age and then progressively form tau inclusions within the hippocampus, showing memory declines as they age from 2.5 to 4.5 months (Ramsden et al., 2005; SantaCruz et al., 2005). I therefore began administration of FPS-ZM1 at 2 months of age and performed behavioral tests at 4.5 months of age (Figure 2.16.A). As reported, 4.5-month-old vehicle-treated rTg4510 mice showed cognitive deficits in the Y-maze test (Figure 2.16.B), novel object recognition test (Figure 2.16.C) and passive avoidance test (Figure 2.16.D). Notably,

rTg4510 mice injected with FPS-ZM1 exhibited significant retention of spatial and learning memory (Figure 2.16.B-D).

Using AT8 immunohistochemistry, I found that rTg4510 mice developed significant less tau pathology in the hippocampus when treated with FPS-ZM1, while tau pathology in the cortex showed no significant difference (Figure 2.17.A-C). In addition, treatment with FPS-ZM1 significantly decreased nuclear translocation of NF-κB p65, and the levels of IL-1β and TNF-α in the hippocampus of rTg4510 mice (Figure 2.18.A-D). Together, these results suggest RAGE mediates tau pathology progression by promoting transsynaptic tau propagation and inflammatory responses, and blocking its function may delay memory impairment in tauopathies.

2.2. Figures

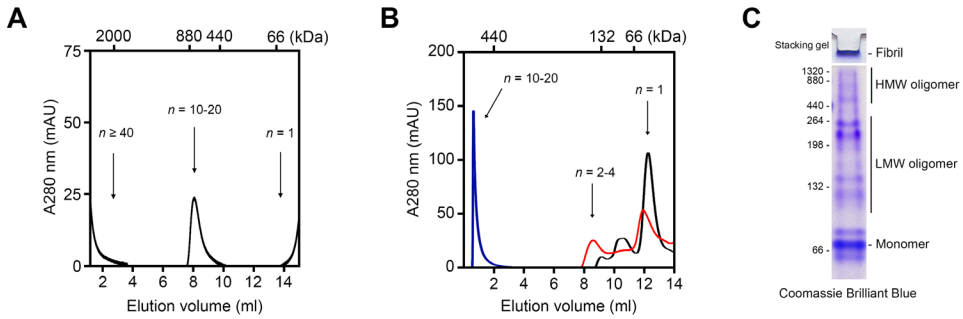

Figure 2.1. Preparation of tau proteins.

(**A** and **B**) Tau monomer was incubated with heparin at 37℃ with agitation for 24 h (A) or incubated with heparin at room temperature without agitation for 1 h (red) or 1.5 h (blue) (B) and analyzed with size exclusion chromatography. (**C**) Monomeric, oligomeric, and fibrillar tau proteins were subjected to native PAGE and stained with Coomassie Brilliant Blue. *n* indicates estimated number of tau monomer equivalent of the peak.

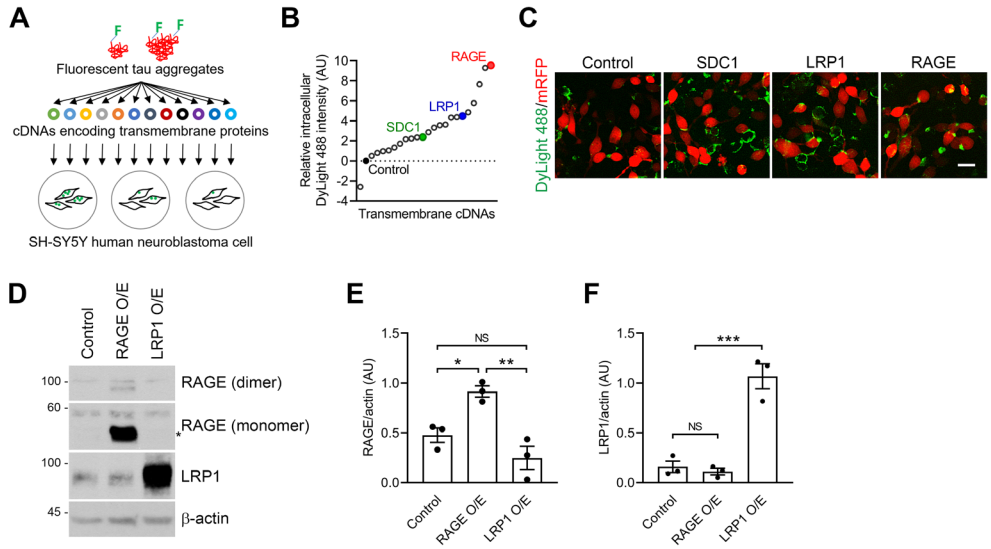

Figure 2.2. Overexpression of RAGE increases cellular tau uptake.

(**A**) Schematic representation of the cell-based tau uptake screen. Cells were transfected with cDNA clones encoding membrane proteins and incubated with DyLight 488-tau aggregates. Extracellular DyLight 488 signals were quenched and cellular tau uptake was visualized. pcDNA3 (Control) and SDC1 were used as negative and positive controls, respectively. (**B** and **C**) From the screen, cellular tau uptake was visualized and mean intracellular DyLight 488 intensities of putative positive clones were measured (n = 3). Scale bar, 10 μm. (**D**) Basal levels of RAGE and LRP1 expression in SH-SY5Y cells were analyzed by immunoblotting following ectopic expression (O/E) of them. Asterisk indicates non-glycosylated form. (**E** and **F**) The levels of RAGE (E) and LRP1 (F) were normalized to β-actin. One-way ANOVA with Tukey test, n = 3. NS, not significant, *P < 0.05, **P < 0.01, ***P < 0.001. Data are represented as mean ± SEM.

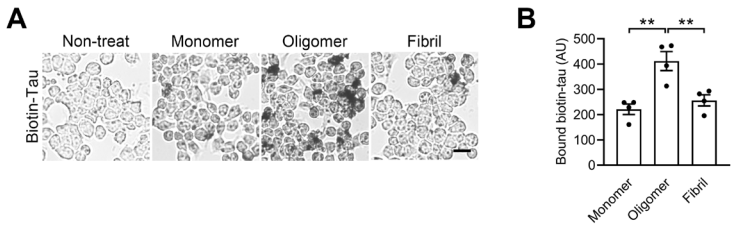

Figure 2.3. RAGE preferentially binds to tau oligomers.

(**A**) SH-SY5Y cells were left untreated or treated with biotin-tau proteins. Scale bar, 20 μm. (**B**) Cell-bound biotin signal intensities were measured and normalized to that from untreated cells. One-way ANOVA with Tukey test, $n = 4$, $^{**}P < 0.01$. Data are represented as mean ± SEM.

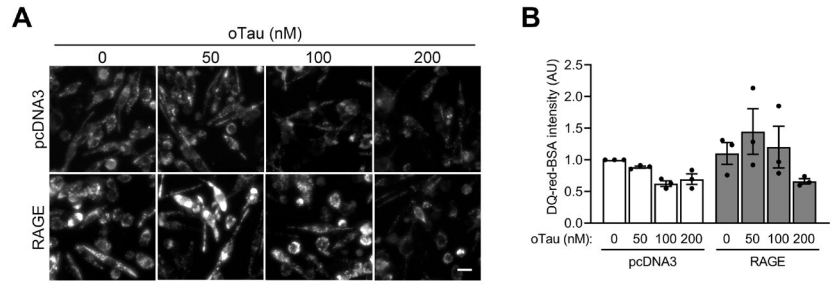

Figure 2.4. Overexpression of RAGE increases lysosomal activity.

(**A**) SH-SY5Y cells were transfected with pcDNA3 or RAGE cDNA for 24 h and then treated with indicated concentrations of tau oligomers. After 24 h, lysosomal activities were imaged using DQ-red-BSA. Scale bar, 10 μm. (**B**) Quantification of the DQ-red-BSA intensities (n = 3). Data are represented as mean ± SEM.

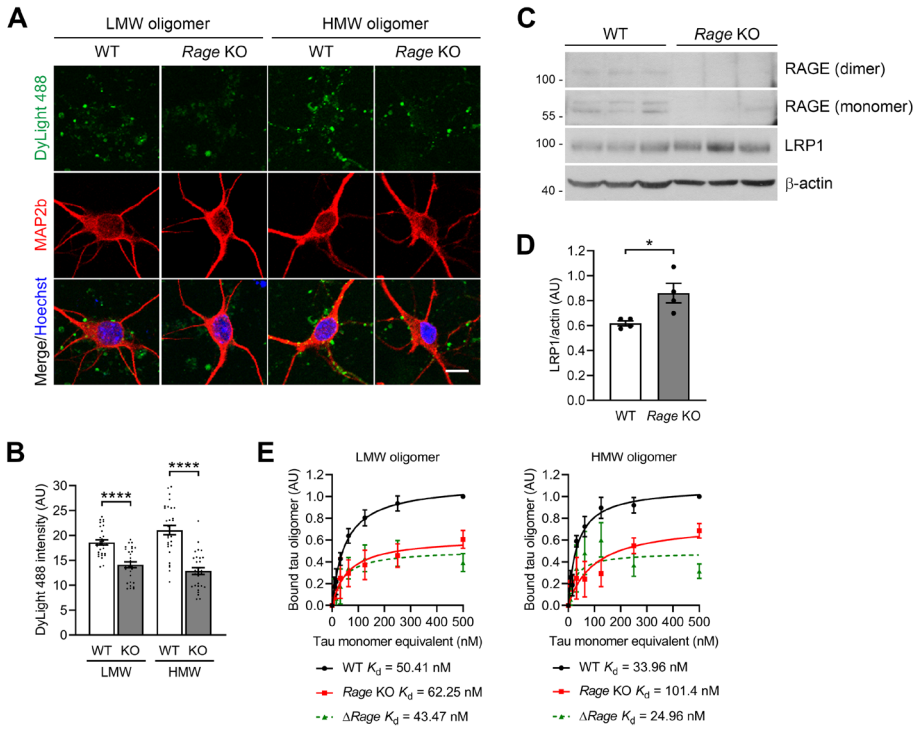

Figure 2.5. *Rage* deficiency reduces neuronal tau uptake.

(**A**) Primary cortical neurons were treated with DyLight 488-tau oligomers and tau uptake was visualized. Scale bar, 10 μm. (**B**) Quantification of the intracellular DyLight 488 signal intensities. Unpaired *t*-test, two-tailed, 30 cells per group, $n = 4$, ****$P < 0.0001$. (**C**) Basal levels of RAGE and LRP1 expression in primary cortical neurons were analyzed by immunoblotting. (**D**) The levels of LRP1 were normalized to β-actin. Unpaired *t*-test, two-tailed, $n = 4$ per group. *$P < 0.05$. (**E**) Primary cortical neurons were treated with biotin-LMW (left) or HMW (right) tau oligomers and cell-bound biotin signal intensities were measured. The dissociation constants (K_d) of the tau binding to RAGE (Δ*Rage* K_d) were obtained (LMW, $n = 6$; HMW, $n = 4$). Data are represented as mean ± SEM.

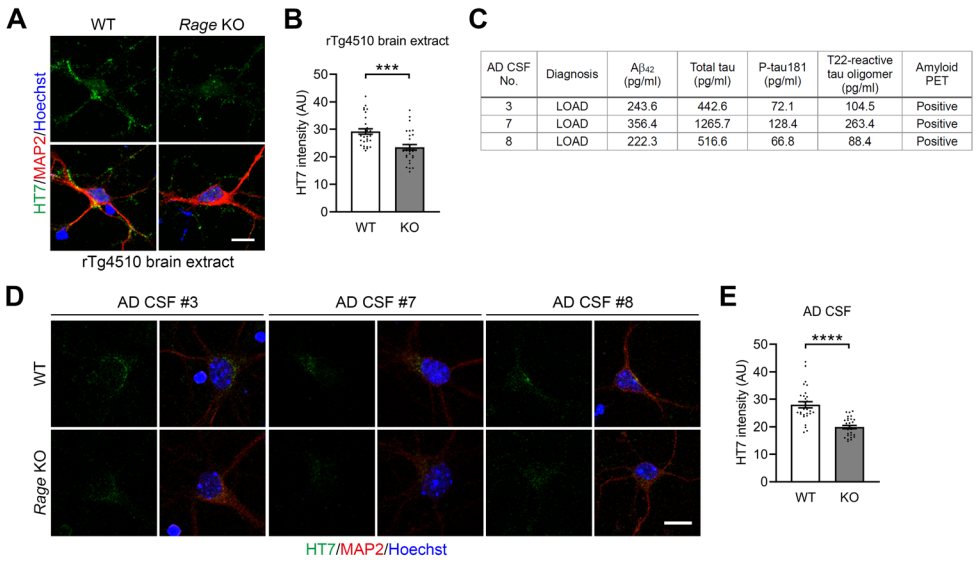

AD CSF No.	Diagnosis	$A\beta_{42}$ (pg/ml)	Total tau (pg/ml)	P-tau181 (pg/ml)	T22-reactive tau oligomer (pg/ml)	Amyloid PET
3	LOAD	243.6	442.6	72.1	104.5	Positive
7	LOAD	356.4	1265.7	128.4	263.4	Positive
8	LOAD	222.3	516.6	66.8	88.4	Positive

Figure 2.6. RAGE mediates accumulation of pathological tau.

(**A**) Primary cortical neurons were incubated with PBS-soluble brain extracts from 12-month-old rTg4510 mice (50 ng/ml human tau). (**B**) Quantification of intracellular human tau intensities. Mann-Whitney test, two-tailed, 30 cells per group, $n = 3$, $^{***}P < 0.001$. (**C**) Clinical information on the AD CSF samples used in this study. LOAD, late-onset AD. (**D**) Primary cortical neurons were treated for 24 h with 1:20 diluted AD CSF and the intracellular human tau intensities were measured. Mann-Whitney test, two-tailed, 30 cells per group, $n = 3$. $^{****}P < 0.0001$. Scale bars, 10 μm. Data are represented as mean ± SEM.

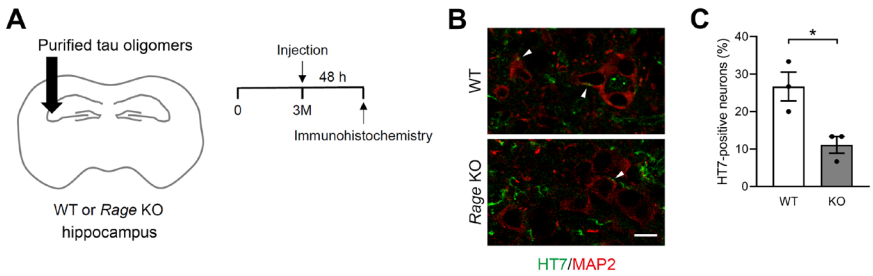

Figure 2.7. *Rage* deficiency reduces neuronal tau uptake in mouse hippocampus.

(**A**) Schematic representation of *in vivo* tau uptake assays. The 3-month-old mice were intracranially injected with purified tau oligomers into the hippocampus. (**B**) After 48 h, brain sections from the hippocampus were immunostained with anti-human tau (HT7) and anti-MAP2 antibodies. Arrowheads, intracellular tau. Scale bar, 10 μm. (**C**) Percentages of HT7-positive neurons in the injection area. Unpaired *t*-test, two-tailed, $n = 3$ per group. *$P < 0.05$. Data are represented as mean ± SEM.

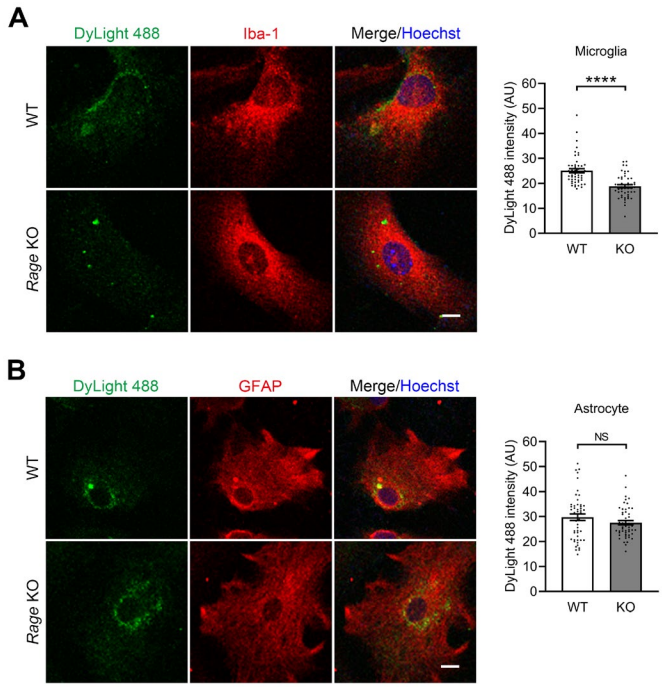

Figure 2.8. *Rage* deficiency reduces tau uptake in microglia but not in astrocytes.

(**A** and **B**) Mouse primary microglia (A) and astrocytes (B) were treated with DyLight 488-tau oligomers. Cellular tau uptake was visualized (left) and the intracellular DyLight 488 signal intensities were measured (right, Mann-Whitney test, two-tailed test, 50 cells per group, $n = 4$. NS, not significant, ****$P < 0.0001$). Scale bar, 10 μm. Data are represented as mean ± SEM.

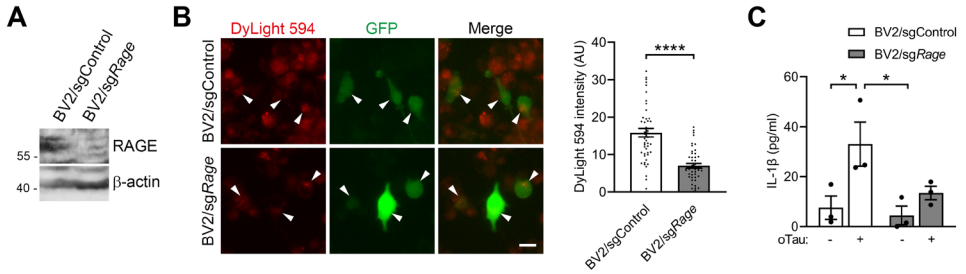

Figure 2.9. RAGE mediates inflammatory cytokine secretion in BV2 mouse microglia cells.

(**A**) Levels of RAGE in BV2/sgControl and BV2/sg*Rage* cells were analyzed by immunoblotting. (**B**) BV2 cells were transfected with pEGFP-N1 and treated with DyLight 594-tau oligomers. Cellular tau uptake was visualized (left) and the intracellular DyLight 594 signal intensities were measured (right). Arrowheads, intracellular tau. Scale bar, 10 μm. Mann-Whitney test, two-tailed, 48 cells per group, $n = 3$. ****$P < 0.0001$. (**C**) The levels of IL-1β in cell conditioned medium were measured by ELISA after the treatment of DyLight 594-tau oligomers for 24 h. Two-way ANOVA with Tukey test, $n = 3$, *$P < 0.05$. Data are represented as mean ± SEM.

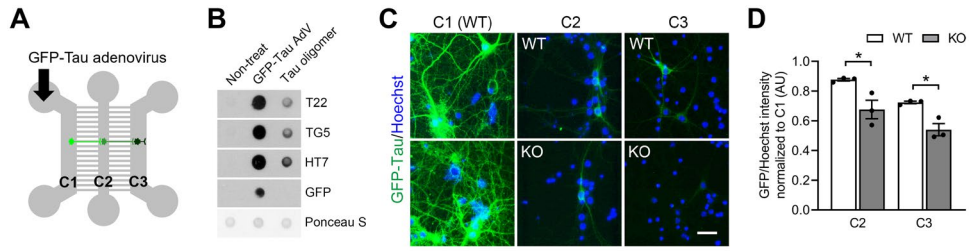

Figure 2.10. *Rage* deficiency reduces transsynaptic tau propagation.

(**A**) Schematic representation of the three-chamber microfluidic device used for *in vitro* tau propagation assays. Neurons in the C1 were transduced with a GFP-tau adenovirus for tau oligomer formation. (**B**) Primary hippocampal neurons were left untreated, transduced with GFP-tau adenovirus (GFP-tau AdV), or treated with tau oligomers. Formation of intracellular tau aggregates was assessed with dot blot assays. (**C**) The propagation of GFP-tau from C1 to C2 and C3 neurons was detected. Scale bar, 20 μm. (**D**) Quantification of the GFP signal intensities from the chambers. Unpaired *t*-test, two-tailed, $n = 3$, $^*P < 0.05$. Data are represented as mean ± SEM.

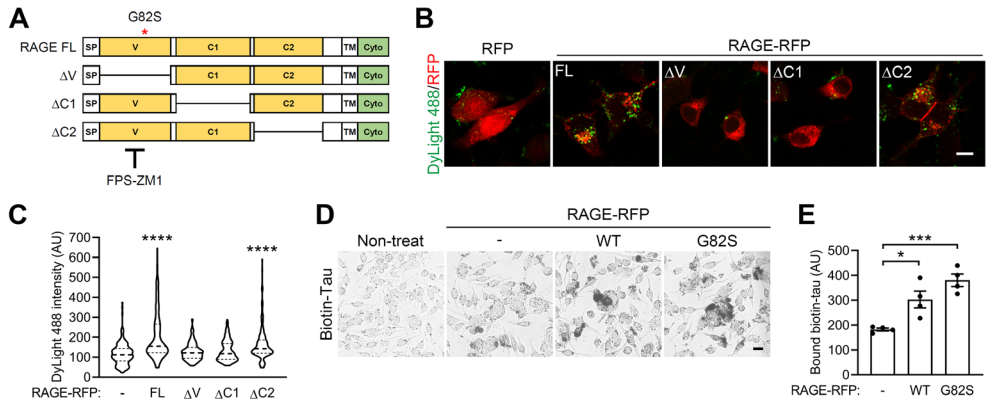

Figure 2.11. RAGE V-C1 domains mediate tau uptake.

(**A**) Schematic representations of RAGE full-length (FL), mutants lacking extracellular ligand-binding domains (ΔV, ΔC1 and ΔC2), and a functional single-nucleotide polymorphism (G82S). FPS-ZM1 binds specifically to the V domain. SP: signal peptide, V: Ig-like V-type domain, C1: Ig-like C2-type 1 domain, C2: Ig-like C2-type 2 domain, TM: transmembrane region, Cyto: cytoplasmic domain. (**B**) SH-SY5Y cells were transfected with RFP or RAGE-RFP and incubated with DyLight 488-tau oligomers. Cellular tau uptake was visualized. (**C**) Quantification of the intracellular DyLight 488 signal intensities. Data are represented as violin plots depicting median and quartiles. Kruskal-Wallis test with Dunn's test, 180 cells per group, $n = 3$. ****$P < 0.0001$. (**D**) SH-SY5Y cells were transfected with RFP or RAGE-RFP and left untreated or treated with biotin-tau oligomers. (**E**) Cell-bound biotin signal intensities were measured and normalized to that from untreated cells. One-way ANOVA with Tukey test, $n = 4$, *$P < 0.05$, ***$P < 0.001$. Data are represented as mean ± SEM. Scale bars, 10 μm.

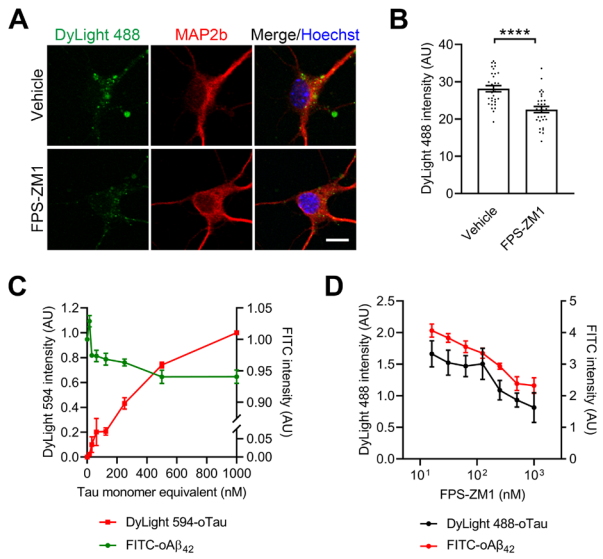

Figure 2.12. Blocking RAGE V domain reduces tau uptake.

(**A**) Primary cortical neurons were treated with DyLight 488-tau oligomers in the presence of 1 μM FPS-ZM1. Scale bar, 10 μm. (**B**) Quantification of the intracellular DyLight 488 signal intensities. Unpaired *t*-test, two-tailed, 40 cells per group, $n = 3$. ****$P < 0.0001$. (**C**) SH-SY5Y cells overexpressing RAGE were co-treated with 125 nM FITC-Aβ$_{42}$ oligomers (green) and increasing concentrations of DyLight 594-tau oligomers (red). After 2 h, the intracellular DyLight 594 and FITC intensities were measured ($n = 3$). (**D**) SH-SY5Y cells were treated with the increasing concentrations of FPS-ZM1 in the presence of 500 nM DyLight 488-tau or 125 nM FITC-Aβ$_{42}$ oligomers and the intracellular DyLight 488 and FITC intensities were measured ($n = 4$). Data are represented as mean ± SEM.

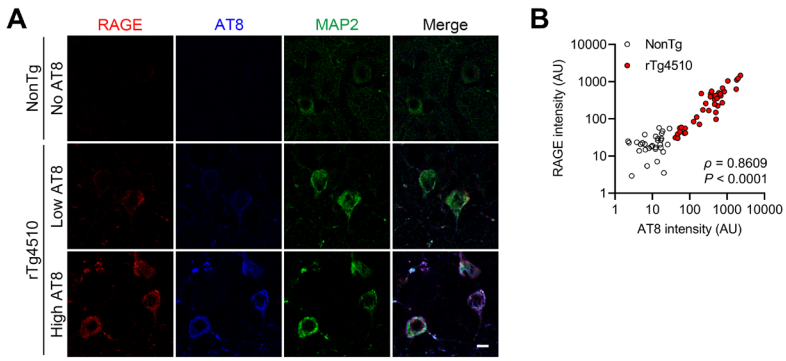

Figure 2.13. Neuronal RAGE expression level increases in the hippocampus of rTg4510 mice.

(**A**) Brain sections from the hippocampus of 4.5-month-old NonTg and age-matched rTg4510 mice were immunostained. Scale bar, 10 μm. (**B**) Scatter plot displaying correlation between RAGE and phospho-tau (AT8) levels in the hippocampal neurons from 4.5-month-old NonTg and age-matched rTg4510 mice. Data was analyzed with Pearson correlation test (NonTg, 35 cells; rTg4510, 40 cells; n = 5 per group).

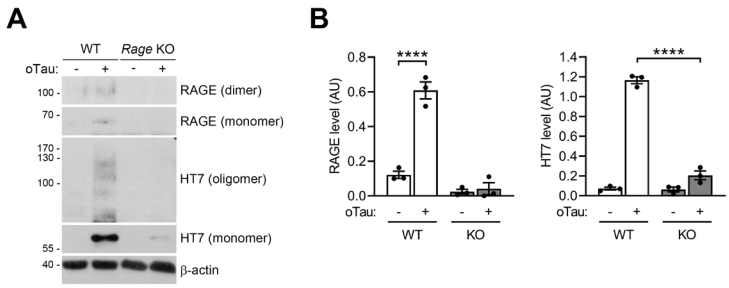

Figure 2.14. Extracellular tau oligomers increase RAGE expression levels in neurons.

(**A**) Primary cortical neurons were treated for 48 h with tau oligomers and analyzed by immunoblotting. (**B**) The relative levels of RAGE (left) and human tau (right) were normalized to β-actin. Two-way ANOVA with Bonferroni test, $n = 3$, ****$P < 0.0001$. Data are represented as mean ± SEM.

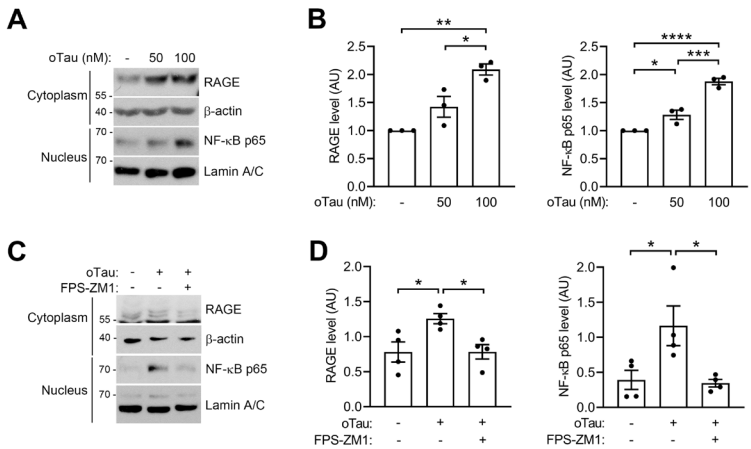

Figure 2.15. Tau oligomers upregulate RAGE expression levels via NF-κB pathway.

(**A**) SH-SY5Y cells were treated for 48 h with tau oligomers. Cytoplasmic RAGE expression and nuclear NF-κB p65 levels were analyzed by immunoblotting. (**B**) The relative level of cytoplasmic RAGE was normalized to β-actin (left) and the relative level of nuclear NF-κB p65 was normalized to Lamin A/C (right). One-way ANOVA with Tukey test, $n = 3$, $^{*}P < 0.05$, $^{**}P < 0.01$, $^{***}P = 0.001$, $^{****}P < 0.0001$. (**C**) SH-SY5Y cells were treated for 48 h with tau oligomers in the presence of 1 μM FPS-ZM1. Cytoplasmic RAGE expression and nuclear NF-κB p65 levels were analyzed by immunoblotting. (**D**) The relative level of cytoplasmic RAGE was normalized to β-actin (left) and the relative level of nuclear NF-κB p65 was normalized to Lamin A/C (right). One-way ANOVA with Tukey test, $n = 4$, $^{*}P < 0.05$. Data are represented as mean ± SEM.

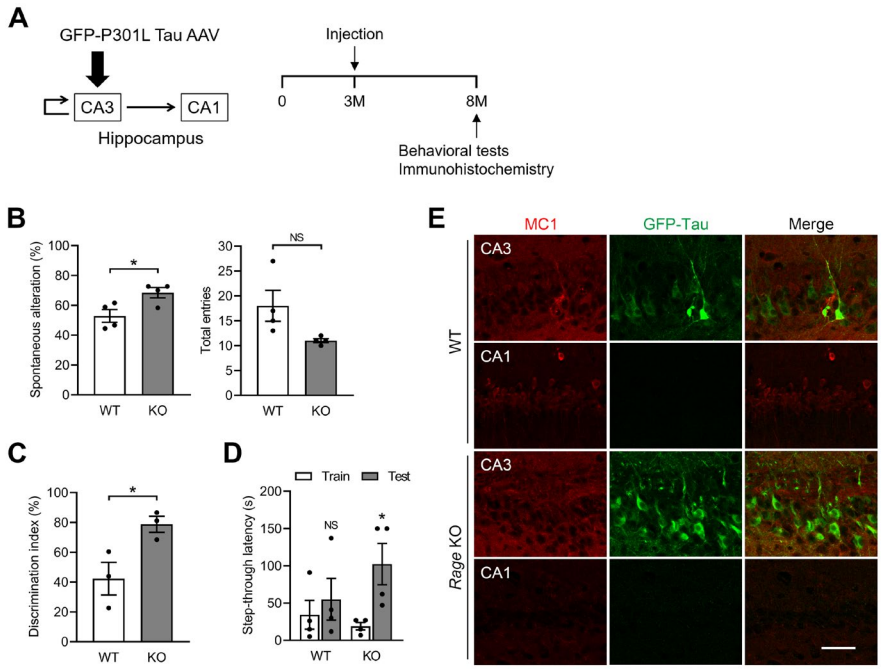

Figure 2.16. *Rage* deficiency delays cognitive impairment induced by viral expression of tau in the hippocampus.

(**A**) Schematic representation of *in vivo* tau propagation. The left hippocampus of 3-month-old mice (male) was intracranially injected with GFP-P301L tau adeno-associated virus ($6.5x10^{10}$ ifu/ml, 5 μl). (**B-D**) After 5 months of injection, mice were analyzed with the Y-maze test (B, unpaired *t*-test, two-tailed, $n = 4$ per group), novel object recognition test (C, unpaired *t*-test, two-tailed, $n = 3$ per group) or passive avoidance test (D, paired *t*-test, two-tailed, $n = 4$ per group). NS, not significant, $*P < 0.05$. (**E**) After behavioral tests, brain sections from the hippocampus were immunostained with anti-misfolded tau (MC1) and anti-MAP2 antibodies. Data are represented as mean ± SEM.

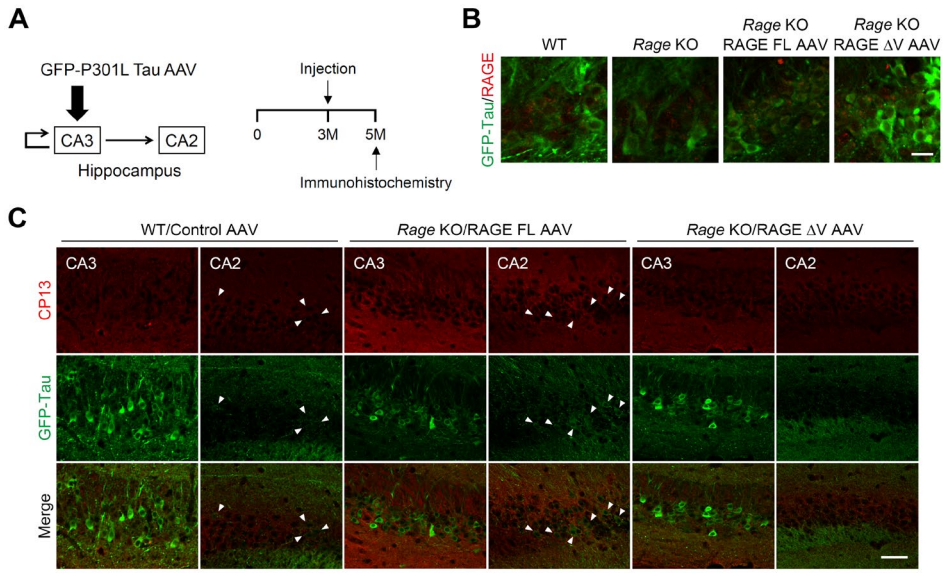

Figure 2.17. Neuronal RAGE mediates tau propagation from the hippocampal CA3 to CA2 neurons *in vivo.*

(**A**) Schematic representation of *in vivo* tau propagation assays. The hippocampus of 3-month-old mice (male) was intracranially injected with GFP-P301L tau AAV ($6.5x10^{10}$ ifu/ml, 5 μl), followed by intracerebroventricular injection of Control AAV ($1.8x10^{13}$ GC/ml) in WT mice, and RAGE FL AAV ($1.93x10^{13}$ GC/ml, 10 μl) or RAGE ΔV AAV ($2.13x10^{13}$ GC/ml, 10 μl) in *Rage* KO mice. (**B**) After 5 weeks of RAGE FL or ΔV AAV injection, brain sections prepared from the hippocampal tissues were immunostained (RAGE, red). Scale bar, 20 μm. (**C**) After 8 weeks of the GFP-P301L tau AAV injection, brain sections prepared from the hippocampal tissues were immunostained with anti-phospho tau (CP13) antibody and examined for GFP-P301L tau propagation (n = 3 per group). Arrowheads, GFP-tau. Scale bar, 50 μm.

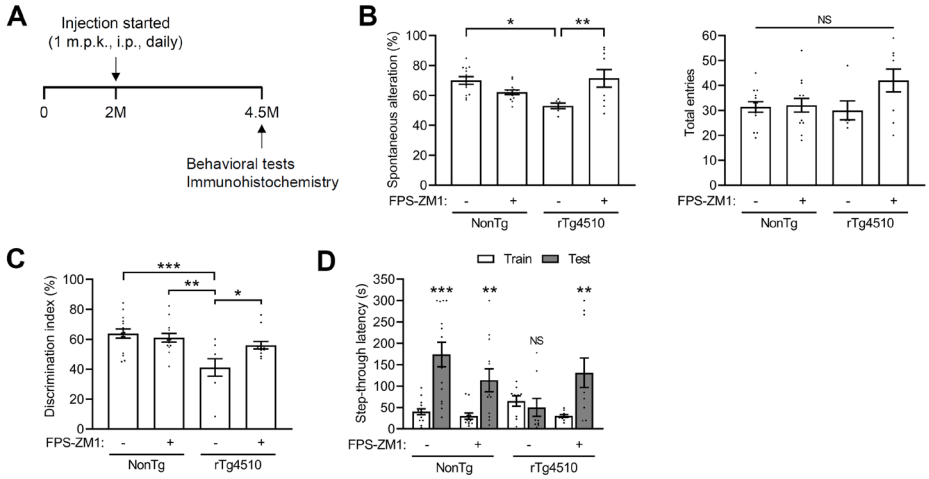

Figure 2.18. RAGE antagonist FPS-ZM1 treatment alleviates cognitive impairment in rTg4510 mice.

(**A**) The 2-month-old mice were intraperitoneally injected with vehicle or blood-brain barrier permeant RAGE antagonist FPS-ZM1 daily for 2.5 months. (**B-D**) The mice injected with vehicle or FPS-ZM1 were analyzed with the Y-maze test [B, two-way ANOVA with Tukey test. n = 13 (8 males and 5 females), 13 (6 males and 7 females), 6 (2 males and 4 females), 9 (3 males and 6 females)], novel object recognition test [C, two-way ANOVA with Tukey test. n = 15 (8 males and 7 females), 13 (6 males and 7 females), 8 (3 males and 5 females), 12 (5 males and 7 females)] or passive avoidance test [D, Wilcoxon test, two-tailed. n = 14 (8 males and 6 females), 12 (6 males and 6 females), 9 (2 males and 7 females), 10 (4 males and 6 females)]. NS, not significant, *P < 0.05, **P < 0.01, ***P < 0.001. Data are represented as mean ± SEM.

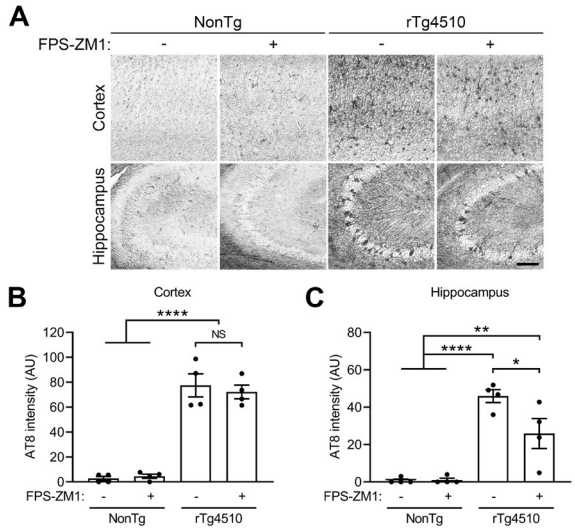

Figure 2.19. Tau pathology progression is decreased in the rTg4510 mice after FPS-ZM1 treatment.

(**A**) Brain sections were prepared from mice injected with vehicle or FPS-ZM1 and immunostained with phospho-tau (AT8) antibody. Scale bar, 100 μm. (**B** and **C**) AT8 signal intensities in the cortex (B) and hippocampus CA3 region (C) were quantified. Two-way ANOVA with Tukey test, $n = 4$ per group. NS, not significant, *$P < 0.05$, **$P < 0.01$, ****$P < 0.0001$. Data are represented as mean ± SEM.

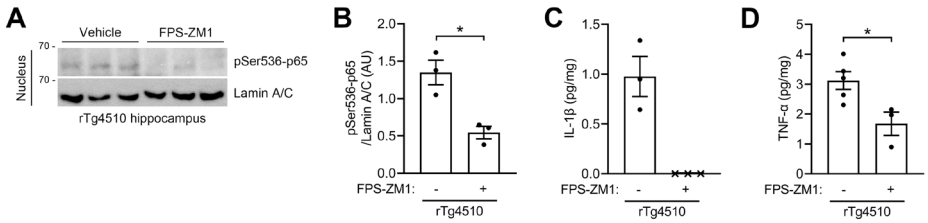

Figure 2.20. RAGE antagonist FPS-ZM1 treatment decreased inflammatory responses in the rTg4510 mice.

(**A**) Nuclear fractions of the hippocampal extracts were prepared form rTg4510 mice after treatment with vehicle or FPS-ZM1 for 2.5 months. Levels of nuclear NF-κB pSer536-p65 were analyzed by immunoblotting. (**B**) The levels of nuclear NF-κB pSer536-p65 were normalized to Lamin A/C. Unpaired *t*-test, two-tailed, $n = 3$ per group. (**C** and **D**) The levels of IL-1β (C) and TNF-α (D) were measured in the hippocampal extracts of 4.5-month-old rTg4510 mice after treatment with vehicle (-) or FPS-ZM1. $n = 3$ per group, X, not detected (C). Unpaired *t*-test, two-tailed, $n = 5, 3$ (D). $^*P < 0.05$. Data are represented as mean ± SEM.

2.3. Materials and Methods

Recombinant tau purification, fluorescence labelling and fibrillation

Human 0N4R tau was subcloned into pET-6xHis vector as previously described (Kim et al., 2016), expressed in BL21-DE3, and purified using Ni-NTA agarose (Qiagen). Tau monomer was incubated with DyLight 488 or 594 NHS Ester (Thermo Fisher Scientific) for fluorescence labelling. For tau oligomer preparation, 24 μM tau monomer was incubated with 5 mM dithiothreitol (DTT) and 6 μM heparin in PBS, and the mixture was incubated for 1 h (low-molecular-weight) or 1.5 h (high-molecular-weight) at room temperature without agitation. Tau fibrils were prepared by incubating the mixture for 24 h at 37℃ under agitation at 1,000 rpm. The molecular sizes of tau oligomers and fibrils were determined by fast protein liquid chromatography (FPLC). Briefly, tau proteins were separated through Superose 6 or Superdex 200 Increase 10/300GL columns (GE Healthcare). Fractions were collected and the presence of tau protein was monitored by absorbance at 280 nm. Tau proteins were subjected to native PAGE and stained with Coomassie Brilliant Blue to confirm its molecular sizes.

Plasmid construction

Human RAGE was amplified by PCR from cDNA library and subcloned into pEGFP-N1, 3XFLAG-CMV-14, or pRFP-N1. The target guide sequence of mouse *Rage* was subcloned into lentiCRISPR v2 (a gift from

Feng Zhang, Addgene plasmid #52961) (Sanjana et al., 2014). The deletion (ΔV, ΔC1, and ΔC2) and G82S RAGE mutants and P301L tau mutant were generated by site-directed mutagenesis.

Cell culture and DNA transfection

SH-SY5Y, HEK293T and BV2 cells were maintained in DMEM/high glucose medium (HyClone) containing 10% fetal bovine serum (FBS), 100 U/ml Penicillin-Streptomycin, and 10 μg/ml Gentamicin (Gibco). Cells were grown at 37°C under an atmosphere of 5% CO_2. Cells were transfected using Lipofector-pMAX (AptaBio) or polyethylenimine (Sigma-Aldrich) according to the manufacturer's instruction. BV2 control and *Rage* KO cell lines were generated using CRISPR-Cas9 sgRNA.

Cell-based tau uptake receptor screen using cDNA expression library

SH-SY5Y cells were co-transfected for 24 h with pRFP-N1 and each cDNA encoding human and mouse transmembrane proteins in the mammalian expression vectors (total 1,523). The pcDNA3 and SDC1 cDNA were used as negative and positive controls, respectively. Cells were treated for 6 h with 500 nM DyLight 488-tau aggregates, washed with PBS and extracellular DyLight 488 signals were quenched with 0.05% trypan blue. Cellular uptake of tau aggregates was automatically visualized using INCell Analyzer 2000 (GE Healthcare). Images were obtained from two random

fields of each well and intracellular DyLight 488 signal intensities in the RFP-positive cells were measured using ImageJ.

Generation of *Ager* knockout (*Rage* KO) mice

Ager-deficient mice were generated from the embryos that were obtained from the European Mouse Mutant Archive (EM ID: 02352, LEXKO-2071). The received embryos had deletion between exons 2 through 4 of the *Ager* gene, leaving only one LoxP site. The corresponding nucleotide sequence for LoxP excision region was validated by direct-sequencing analysis (Bionics). The genotyping was performed by PCR analysis using the following primers: forward 5′-AGT GTC CTC AGG TCG GGT GA-3′ and reverse 5′-CCA TCT AAG TGC CAG CTA AGG GTC-3′. Mice were backcrossed and maintained on a C57BL/6N background.

Primary cultures of neurons and microglia

Mouse primary cortical and hippocampal neurons were prepared from embryonic day 16.5. The neurons were plated on culture plates or microfluidic chamber devices coated with poly-L-lysine, and maintained in Neurobasal medium (Gibco) containing 2% B-27 supplement (Gibco), 100 U/ml Penicillin-Streptomycin, 10 μg/ml Gentamicin, and 1% GlutaMAX supplement (Gibco). Mouse primary microglia were prepared from the cortices of postnatal day 1 pups and maintained in DMEM medium

containing 10% FBS, 100 U/ml Penicillin-Streptomycin, and 10 μg/ml Gentamicin.

Cellular binding assay and dissociation constant (K_d) calculation

Purified tau monomer was biotinylated using Ez-Link Sulfo-NHS-LC-Biotinylation kit (Thermo Fisher Scientific) and then fibrillated to form oligomers and fibrils. SH-SY5Y cells were transfected for 24 h with RAGE cDNA and incubated for 2 h with biotin-tau proteins. To estimate K_d values for tau binding to RAGE, mouse primary cortical neurons (DIV 7) were incubated for 24 h with varying concentrations of biotin-tau oligomers. Cells were washed with tris-buffered saline (TBS) and fixed with 4% paraformaldehyde for 20 min. Cells were blocked for 1 h with 10% FBS and 0.1% Triton X-100 in TBS, and incubated for 16 h with streptavidin-alkaline phosphatase conjugate (1:2000, Roche) at 4℃. After washing with TBS, the bound biotin-tau was visualized using BCIP/NBP liquid substrate system (Sigma-Aldrich) for 10 min. Images were obtained using INCell Analyzer 2000 and the cell-bound biotin signal was measured using ImageJ. Estimated K_d values for RAGE-binding were obtained from nonlinear regression analysis of saturation binding using Prism (GraphPad Software).

Tau uptake assay in primary cultured cells

Mouse primary cortical neurons at 7 days *in vitro* (DIV 7) were incubated for 24 h with 500 nM DyLight 488-tau oligomers. HSPG-mediated tau

internalization was blocked by co-treatment with 15 U/ml heparin (Sigma-Aldrich). The effect of RAGE antagonist was assessed by co-treatment with 1 μM FPS-ZM1 (Calbiochem). To examine cellular uptake of pathology-associated tau, neurons were incubated for 24 h with PBS-soluble rTg4510 brain extracts containing 50 ng/ml human tau or with 1:20 diluted CSF prepared from human AD patients. Mouse primary microglia or astrocytes (DIV 14) were incubated for 24 h with 100 nM DyLight 488-tau oligomers. Cells were washed with PBS, fixed with 4% paraformaldehyde, and processed for immunocytochemistry. Images were obtained using confocal laser scanning microscopy LSM700 (Carl Zeiss) and intracellular tau signal intensities were measured using ImageJ.

Preparation of rTg4510 brain extracts

The rTg4510 mice were obtained by crossing the human P301L tau responder line (The Jackson Laboratory, #015815) to a tetracycline-controlled transactivator (tTA) line (The Jackson Laboratory, #016198). The 12-month-old rTg4510 mice (male and female) were anesthetized with a mixture of tiletamine/zolazepam (30 mg/kg) and xylazine (10 mg/kg), and perfused with PBS containing 10 U/ml heparin. The brains were excised, frozen in liquid nitrogen, and homogenized in five volumes (wt/vol) of PBS. The homogenates were centrifuged at 3,000 x*g* for 5 min at 4°C. The supernatants were collected and the concentration of human tau was

determined using human tau (total) ELISA kit (Invitrogen) according to the manufacturer's instruction.

Cerebrospinal fluid (CSF) collection from human patients with AD

Human CSF was obtained from a routine lumbar puncture in the L3/L4 or L4/L5 interspace between 8 am to 12 pm. The first 4 ml was used for routine analyses including cell count, protein, and sugar levels. Within 4 h from the lumbar puncture, CSF was centrifuged at 2,000 x*g* for 10 min, and the supernatants were stored at −80°C until use. The levels of CSF $A\beta_{42}$, total tau, and phospho-tau181 (triple marker) were measured by INNOTEST β-$AMYLOID_{(1–42)}$, hTAU Ag and $PHOSPHO\text{-}TAU_{(181P)}$ ELISA kits (Fujirebio Europe, Gent, Belgium) according to the manufacturer's instructions. The levels of CSF tau oligomer were measured following the previous report with modification (Sengupta et al., 2017). Briefly, 10 µl human CSF samples in PBS were coated in 96-well plate (Corning Costar 9018) overnight at 4℃. Plate was washed with PBS containing 0.05% Tween-20 (PBS-T) and blocked with ELISA/ELISPOT (Invitrogen) for 2 h at room temperature. After washing with PBS-T, 100 µl anti-oligomeric tau T22 antibody (Merck, 1:250) was added and incubated overnight at 4℃. After washing with PBS-T, HRP-conjugated anti-rabbit IgG (Jackson ImmunoResearch Laboratories,1:3000) was added and incubated overnight at 4℃. After washing with PBS-T, plate was developed with 1X TMB

Solution (Invitrogen) for 10 min and read at 450 nm. The serial dilutions of T22-reactive purified tau oligomer were used for generating standard curve of the assay. The T22-reacive tau was separated by gradient ultracentrifugation with 5-20% glucose gradient and 0-0.2 % glutaraldehyde.

Tau uptake in mouse hippocampus

The 3-month-old mice (male) were anesthetized with a mixture of tiletamine/zolazepam (30 mg/kg) and xylazine (10 mg/kg), and intracranially injected with 6 μg of purified tau oligomers into the hippocampus (stereotaxic coordinates: anteroposterior = –2.1 mm, mediolateral = 1.8 mm, and dorsoventral = –2.0 mm from bregma) using 30-gauge Hamilton microsyringe. After 48 h, mice were anesthetized and perfused with PBS containing 10 U/ml heparin and 4% paraformaldehyde. Brain sections (40 μm) were prepared from the hippocampus and processed for immunohistochemistry. Images were obtained using confocal laser scanning microscopy LSM700 and counted for human tau-positive cells in the injection area.

Measurement of inflammatory cytokines in cell conditioned medium and mouse brain tissues

For inflammatory cytokine measurement, BV2/sgControl and BV2/sg*Rage* cells were transfected for 24 h with pEGFP-N1. Cells were then treated for 24 h with 125 nM DyLight 594-tau oligomers and cell conditioned medium was stored for ELISA assay. Cells were washed with PBS, and cellular uptake of tau oligomers was visualized under fluorescence microscope. Intracellular DyLight 594 signal intensities in GFP-positive cells were measured using ImageJ. The hippocampal tissues from rTg4510 mice treated with vehicle or FPS-ZM1 for 2.5 months were prepared, and cytoplasmic fraction of the tissue extract was subjected to ELISA assay. The levels of IL-1β and TNF-α were measured by Quantikine Mouse IL-1β/IL-1F2 ELISA kit (R&D Systems) and Mouse TNF alpha ELISA kit (Invitrogen), respectively, according to manufacturer's instruction.

Generation of recombinant adenovirus and adeno-associated virus

A recombinant adenovirus was generated as described previously (Park et al., 2012). A recombinant adeno-associated virus (AAV) vector was generated by subcloning GFP-P301L tau into the pJDK viral vector (kindly gifted from Dr. H. Lee, University of Ulsan College of Medicine). Viral production was performed using HEK293T cells and monitored under fluorescence microscopy. Cells were harvested, lysed by freeze–thawing, and viral particles were purified by CsCl gradient centrifugation or using AAVpro Purification Kit (Takara Bio) according to the manufacturer's instruction. Concentration of infectious viral particles was estimated by

infection of cells with serial dilutions of virus and counting GFP-positive cells using BD FACSCanto II (BD Biosciences).

Tau propagation assay using three-chamber microfluidic device

Microfluidic devices were prepared by fabricating of poly(dimethylsiloxane) (Sylgard 184, Dow Corning) on the master mold (kindly gifted by Dr. N. L. Jeon, Seoul National University), and bonding with poly-L-lysine-coated slides as previously described (Park et al., 2006). Mouse primary hippocampal neurons were cultured in the three chambers of the device: WT neurons in the 1st chamber and WT or *Rage* KO neurons in the 2nd and 3rd chambers. WT neurons in the 1st chamber (DIV 7) were transduced for 24 h with GFP-tau adenovirus ($0.76x10^8$ TU/ml, MOI 50). Chambers were fluidically isolated from each other by establishing 50 μl volume differences, thereby restricting the diffusion across the chambers. After 14 days, neurons in the chambers were washed with PBS, fixed with 4% paraformaldehyde, and nucleus was visualized with Hoechst 33342 (Sigma-Aldrich). Images were obtained using fluorescence microscope (Olympus) and tau propagation across chambers was compared by measuring intracellular GFP intensities of the chambers using ImageJ.

Dot blot assay

Mouse primary hippocampal neurons (DIV 7) were transduced for 24 h with GFP-Tau adenovirus ($0.76x10^8$ TU/ml, MOI 10) or incubated for 24 h with 500 nM tau oligomers. After 48 h, cell lysates were prepared in 1% SDS

lysis buffer and filtered through 0.2 μm nitrocellulose membrane using 96-well vacuum dot blot apparatus (Bio-Rad). The membrane was stained with Ponceau S to indicate total protein loading, washed with TBS containing 0.05% Tween 20 (TBS-T), blocked for 1 h with 5% non-fat milk in TBS-T, and analyzed by immunoblotting.

Preparation of $A\beta_{42}$ oligomers

The synthetic FITC-$A\beta_{42}$ peptide (rPeptide) was solubilized in DMSO and oligomers were prepared as described previously (Kam et al., 2013). The synthetic biotin-$A\beta_{42}$ peptide (rPeptide) was dissolved in DMSO at 2 mM and diluted in PBS to obtain a 100 μM stock solution. After incubating for 16 h at 22℃, the preparation was centrifuged at 16,000 x*g* for 15 min, the supernatant was collected, and were stored at −80°C until use.

***In vivo* tau propagation using AAV system**

The 3-month-old mice (male) were anesthetized with a mixture of tiletamine/zolazepam (30 mg/kg) and xylazine (10 mg/kg), and intracranially injected with 5 μl GFP-P301L tau AAV ($6.5x10^{10}$ ifu/ml) into the left hippocampus (stereotaxic coordinates: anteroposterior = –2.1 mm, mediolateral = 1.8 mm, and dorsoventral = –2.0 mm from bregma) using 30-gauge Hamilton microsyringe at the rate of 0.5 μl/min. After 20 weeks, mice were analyzed with behavioral tests. For neuronal RAGE

reconstitution experiment, full-length (FL) and ΔV mutant RAGE were subcloned into the AAV vector with CaMKIIa promoter and their AAVs were purified (KIST Virus Facility). After 3 weeks of GFP-P301L tau AAV injection, WT mice were subsequently injected with 10 μl Control AAV ($1.8x10^{13}$ GC/ml), and *Rage* KO mice were injected with 10 μl RAGE FL AAV ($1.93x10^{13}$ GC/ml) or RAGE ΔV AAV ($2.13x10^{13}$ GC/ml) into the cerebral ventricle. Mice were then anesthetized and perfused with PBS containing 10 U/ml heparin and 4% paraformaldehyde. Brain sections (40 μm) were prepared from the hippocampus and processed for immunohistochemistry. Images were obtained using confocal laser scanning microscopy LSM700.

Behavioral tests

The 2-month-old non-transgenic mice and their rTg4510 littermates (male and female) were intraperitoneally injected with vehicle (5% DMSO) or FPS-ZM1 (1 mg/kg/day) daily for 2.5 months. The mice were then analyzed with Y-maze, novel object recognition, and passive avoidance tests.

Y-maze test - Mice were placed in the end of one arm of Y-shaped maze (32.5 cm length x 15 cm height) and allowed to move freely for 7 min. An entry into the arm was counted when the whole body including tail is placed in the arm. The percentage of spontaneous alterations was estimated as the ratio of the number of alterations to the total number of entries.

Novel object recognition test - Mice were placed in the chamber (30 cm length x 30 cm width x 25 cm height) to move freely for 7 min at 24 h intervals. Before the test period, mice were habituated in the empty chamber for 2 days. During 3 days of test period, two objects were placed in the chamber and one of the objects were changed every day (novel object) while the other kept unchanged (familiar object). The object exploration was defined as mouse sniffing or touching the object with nose towards it. The object discrimination index was estimated as the ratio of the time of exploring a novel object to the total time of exploring objects.

Passive avoidance test - An apparatus with a light and dark compartments (20 x 20 x 20 cm each) separated by a sliding door was used for the test. Mice were placed in the closed light compartment and allowed to move freely for 1 min before opening the door. For conditioning, the latency time for the mice entering the dark compartment was measured and an electric shock (0.25 mA, 2 s) was delivered by the floor grids after closing the door. For the test, mice were placed in the closed light compartment 24 h after conditioning, allowed to move freely for 1 min before opening the door, and the latency time for the mice entering the dark compartment was measured with a 5 min cut-off.

Immunoblotting

For nuclear extraction, cell pellets or brain tissues were resuspended in hypotonic buffer (20 mM Tris-Cl pH 7.4, 10 mM NaCl, 3 mM $MgCl_2$, 0.5%

NP-40) containing 1 mM PMSF. After centrifugation at 3,000 rpm for 10 min at 4℃, supernatants were isolated as a cytoplasmic fraction. Nuclear fraction was prepared by sonication of pellets in cell extraction buffer (10 mM Tris-Cl pH 7.4, 100 mM NaCl, 1% Triton X-100, 0.1% SDS, 0.5% sodium deoxycholate, 10% glycerol, 1 mM EDTA) containing 1 mM PMSF. After centrifugation at 13,000 rpm for 20 min 4℃, supernatants were isolated as a nuclear fraction. Unless indicated otherwise, cell lysates were prepared by sonication in lysis buffer (50 mM Tris-Cl pH 8.0, 150 mM NaCl, 1% Triton X-100, 0.1% SDS, 0.5% sodium deoxycholate, 1 mM EDTA) containing 1 mM PMSF. After centrifugation at 13,000 rpm for 20 min 4℃, supernatants were separated by SDS-PAGE and transferred onto PVDF membranes (ATTO Corporation). The blots were blocked for 1 h with 5% BSA in TBS-T and incubated with primary antibodies in TBS-T overnight at 4℃. After washed with TBS-T, blots were incubated for 1.5 h with peroxidase-conjugated secondary antibodies (Jackson ImmunoResearch Laboratories; 1:40000) and visualized using ECL detection system.

Immunocytochemistry and immunohistochemistry

For immunocytochemistry, cells were washed with PBS and fixed with 4% paraformaldehyde for 20 min. After washing with PBS, cells were blocked for 1 h with 3% BSA in PBS and incubated with primary antibodies in PBS containing 1% BSA overnight at 4℃. Cells were incubated for 1.5 h with

Alexa Flour 488 or 594 secondary antibodies (Jackson ImmunoResearch Laboratories; 1:500) and nucleus was visualized with Hoechst 33342. The coverslips were placed on the slides with mounting medium (Sigma-Aldrich). For immunohistochemistry, brain sections (40 μm) were prepared, washed with PBS, blocked for 1 h with 10% FBS in PBS containing 1% Triton X-100, and incubated with primary antibodies in PBS containing 5% FBS and 0.1% Triton X-100 overnight at 4℃. After washed, sections were incubated for 1.5 h with Alexa Flour 405, 488, or 594 secondary antibodies (Jackson ImmunoResearch Laboratories; 1:500). Otherwise, sections were processed with VECTASTAIN Elite ABC-HRP kit and developed with ImmPACT DAB Substrate (Vector Laboratories). The sections were placed on the slides with mounting medium.

Statistics

All statistical analyses were performed using GraphPad Prism 9 Software. Sample sizes and the number of replicates were described in each figure legends. Normality of data distribution was assessed using the Shapiro-Wilk test and non-parametric tests were used when the data did not meet the assumptions of the parametric tests. Unpaired *t*-test or Mann-Whitney test was performed when comparing two independent groups. One-way ANOVA, two-way ANOVA, or Kruskal-Wallis test with Tukey, Dunnett, or Bonferroni test was performed when comparing multiple groups. Paired *t*-test or Wilcoxon test was performed when analyzing passive avoidance test

data. Spearman correlation test was performed when analyzing expression levels of RAGE and pathologic tau. *P* values were obtained from two-tailed test. No statistical test was used to predetermine sample size.

Study approval

All mice used in this study were maintained in a specific pathogen-free animal facility. All housing, breeding, and procedures were performed according to the Korean Ministry of Food and Drug Safety (MFDS) and approved by Seoul National University Animal Care and Use Committee. This study was approved by the ethics committee of Seoul National University Bundang Hospital and Seoul National University. All participants gave informed consent to the use of clinical data for research purposes.

Chapter 3. TauIR Immunotherapy Suppresses Neuroinflammation and Tau Spread

3.1. Results

Tau oligomers activate TauIR and are internalized into microglia

To determine whether tau is a pathogenic ligand of TauIR in microglia, I assayed for TauIR activation. I used HEK-Blue hTauIR reporter cells which produce secreted embryonic alkaline phosphatase (SEAP) upon the activation of TauIR-NF-κB pathway. When treated HEK-Blue hTauIR cells with recombinant tau (rTau), TauIR activation increased by 20-24 folds compared to negative controls (Figure 3.1). I then blocked TauIR using anti-TauIR antibody, which binds TauIR leucine repeat region 9-12 near the bacterial lipopeptide-binding site (Ahmad & Choi, 2022). Co-treatment of anti- TauIR antibody with rTau significantly reduced TauIR activation in a dose-dependent manner (Figure 3.1).

Previous studies have demonstrated that microglial TauIR activation promotes phagocytosis of misfolded protein aggregates in neurodegenerative diseases (Chen et al., 2006; Reed-Geaghan et al., 2009; Kim et al., 2013). I therefore examined whether TauIR activation promotes tau uptake into microglia. When BV2 mouse microglial cells were treated with DyLight 594-labeled tau oligomers (DyLight 594-oTau), I found that overexpressed TauIR increases cellular uptake of tau oligomers (Figure 3.2.A and B).

Further, I assessed whether *TauIR* knockout (*TauIR* KO) in microglia affected tau uptake. The results revealed that tau uptake was significantly reduced in *TauIR* KO primary cultured microglia compared to wild-type (WT) microglia (Figure 3.3.A and B). In addition, blockade of TauIR using anti-TauIR antibody reduced tau uptake in WT microglia in a dose-dependent manner (Figure 3.4.A and B). Thus, these results suggest that tau oligomers activate TauIR in microglia to promote cellular uptake of tau oligomers into microglia.

Tau binding to microglial TauIR increases inflammatory responses

In Alzheimer's disease, it is known that microglial activation might be neuroprotective through the clearance of pathogenic tau oligomers or be neurotoxic via mediating the inflammatory response (Javanmehr et al., 2022; Paolicelli et al., 2022). To determine whether TauIR activation and subsequent tau uptake in microglia are associated with neuroprotective or detrimental effect, I examined mRNA expression levels of pro-inflammatory cytokines after tau treatment. When THP-1 human monocytic cells were treated with rTau, I found that the mRNA levels of TNF-α, IL-1β, IL-6 and IL-8 were all significantly increased compared to untreated control cells (Figure 3.5.A-D).

However, treatment of THP-1 cells with anti-TauIR antibody in the presence of rTau significantly reduced the mRNA levels of these pro-inflammatory cytokines in a dose-dependent manner (Figure 3.5.A-D).

Therefore, I believe that tau-induced activation of TauIR in microglia plays a role to promote inflammatory responses which may be associated with neurotoxic environment in brain, and confirmed that anti-TauIR antibody effectively protects neuroinflammation in microglia by blocking TauIR activation.

TauIR is required for tau uptake in neurons

The disease progression and clinical symptoms of Alzheimer's disease exhibit a strong correlation with the distribution and spreading of pathological tau inclusions (Braak & Braak, 1991). Recent studies have demonstrated that tau spreads along neural connectivity (Clavaguera et al., 2009; de Calignon et al., 2012; Wu et al., 2013). Since TauIR has also been reported to expressed in neurons as well as in microglia (Tang et al., 2007; Dzamko et al., 2017), I tested whether TauIR mediates tau uptake in neurons for neuronal propagation. When primary cultured mouse hippocampal neurons were incubated with tau oligomers, I found that tau uptake in *TauIR* KO neurons was reduced compared to WT neurons (Figure 3.6.A and B).

In addition, blockade of TauIR using anti-TauIR antibody reduced tau uptake into WT neurons in a dose-dependent manner (Figure 3.7.A and B). More, I assessed whether TauIR plays a role in tau uptake in the mouse brain. When purified tau oligomers were injected into the hippocampus of WT and *TauIR* KO mice, I observed that *TauIR* deficiency blocked tau

uptake into neurons *in vivo* (Figure 3.8.A-C). Together, I propose that TauIR in neurons mediates tau uptake for neuronal transmission in an autonomous manner and TauIR in microglia facilitates tau transmission through enhancing inflammatory responses.

TauIR deficiency alleviates tau pathology progression

To assess direct role of TauIR in tau pathology, I decided to utilize mouse models of AD. I tested whether blocking the function of TauIR could delay tau pathogenesis and cognitive functions in rTg4510 mice (Ramsden et al., 2005; SantaCruz et al., 2005). I crossed rTg4510 mice or its control tetracycline-controlled transactivator (tTA) mice without P301L tau responder with *TauIR* KO mice and performed behavioral tests at 6 months of age. As reported, 6-month-old rTg4510/WT mice showed cognitive deficits in the Y-maze test, novel object recognition test and passive avoidance test (Figure 3.9.A-C). However, the cognitive functions were not impaired in rTg4510/*TauIR* KO mice (Figure 3.10.A-C). These results suggest that TauIR mediates tau pathology progression, including cognitive impairment, in AD.

3.2. Figures

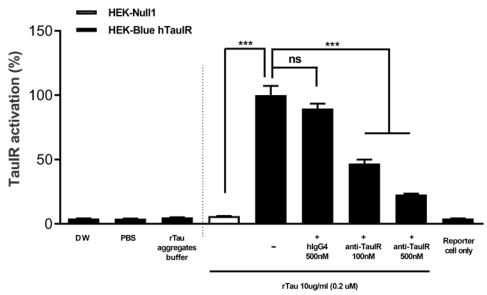

Figure 3.1. **Tau induces TauIR activation.**

HEK-Null1 and HEK-Blue-hTauIR cells were treated rTau (0.2 μM) in the absence or presence of anti-TauIR antibody (100 nM or 500 nM) for 20 h. The secreted levels of SEAP were quantified with the optical density at 620 nm using a microplate reader. One-way ANOVA with Tukey's post-hoc test, ***$P < 0.001$. Data are represented as mean ± SEM.

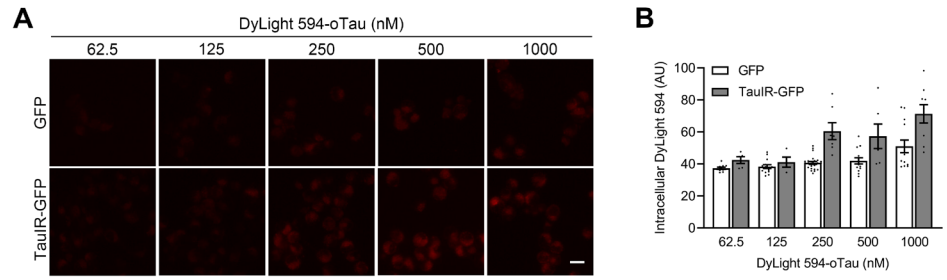

Figure 3.2. **Overexpression of TauIR increases cellular tau uptake.**

(**A**) BV2 cells were transfected with pEGFP-N1 or TauIR-GFP for 24 h and then treated with the increasing concentrations of DyLight 594-tau oligomers for 6 h. After washing, cellular tau uptake was observed under fluorescence microscope. Scale bar, 10 μm. (**B**) Quantification of the intracellular DyLight 594 signal intensities in (A). Data are represented as mean ± SEM.

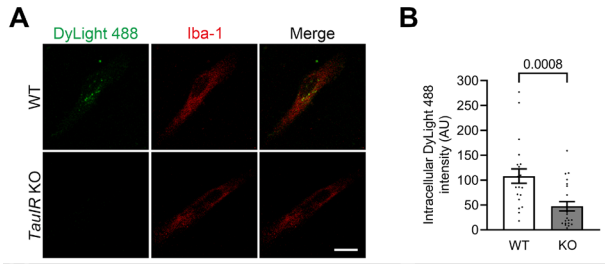

Figure 3.3. *TauIR* deficiency reduces tau uptake in microglia.

(**A**) WT and *TauIR* KO mouse primary microglia (Iba-1) (DIV 14) were treated 125 nM DyLight 488-tau oligomers for 24 h and cellular tau uptake was observed under confocal microscope. Scale bar, 10 μm. (**B**) Quantification of the intracellular DyLight 488 signal intensities in (A). Mann-Whitney test, two-tailed, 21-22 cells per group. Data are represented as mean ± SEM.

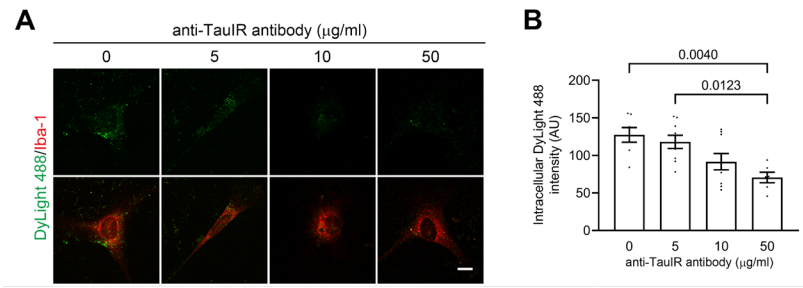

Figure 3.4. Blocking TauIR reduces tau uptake in microglia.

(**A**) Mouse primary microglia (Iba-1) (DIV 14) were pre-treated with or without anti-TauIR antibody for 3 h and then co-treated 100 nM DyLight 488-tau oligomers for 24 h. Cellular tau uptake was observed under confocal microscope. Scale bar, 10 μm. (**B**) Quantification of the intracellular DyLight 488 signal intensities in (A). One-way ANOVA with Tukey's post-hoc test. Data are represented as mean ± SEM.

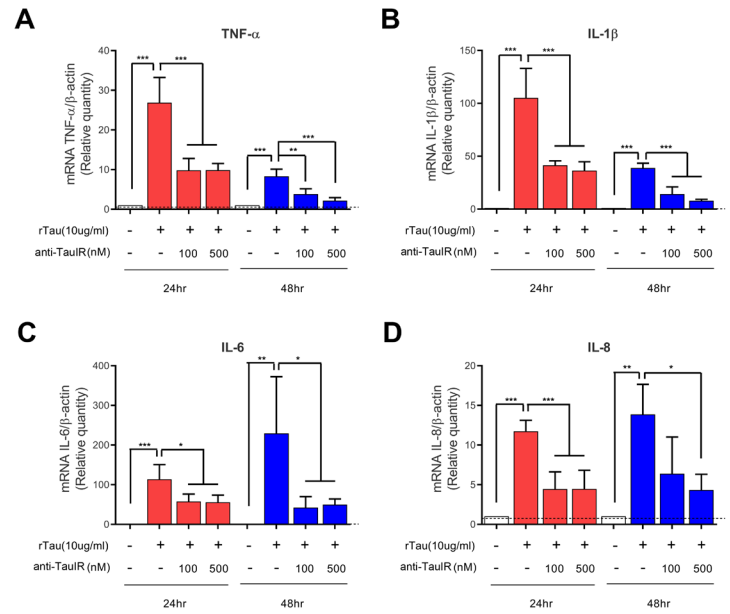

Figure 3.5. Tau induces TauIR activation and inflammatory responses.

(**A-D**) THP-1 cells were treated with 10 μg/ml rTau for 24 h or 48 h in the presence or absence of anti-TauIR antibody (100 nM and 500 nM). The mRNA levels of pro-inflammatory cytokine TNF-α (A), IL-1β (B), IL-6 (C) and IL-8 (D) were measured with qRT-PCR. One-way ANOVA with Tukey's post-hoc test, $*P < 0.05$, $**P < 0.01$, $***P < 0.001$.

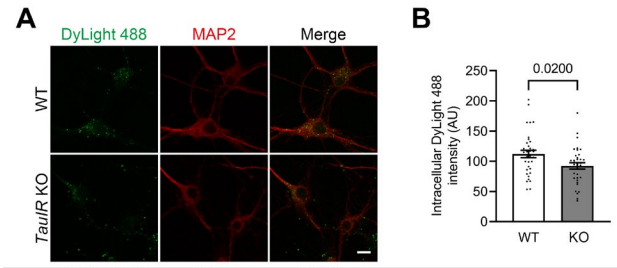

Figure 3.6. TauIR mediates tau uptake in neurons.

(**A**) WT and *TauIR* KO mouse primary hippocampal neurons (MAP2) (DIV 7) were treated 50 nM DyLight 488-tau oligomers for 24 h and cellular tau uptake was then observed under confocal microscope. Scale bar, 10 μm. (**B**) Quantification of the intracellular DyLight 488 signal intensities in (A). Mann-Whitney test, two-tailed, 35 cells per group, n = 3. Data are represented as mean ± SEM.

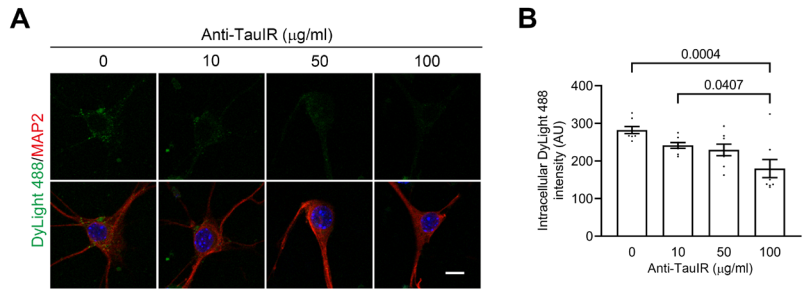

Figure 3.7. Blocking TauIR reduces tau uptake in neurons.

(**A**) Mouse primary hippocampal neurons (MAP2) (DIV 7) were treated 500 nM DyLight 488-tau oligomers with or without anti-TauIR antibody for 24 h and cellular tau uptake was observed under confocal microscope. Scale bar, 10 μm. (**B**) Quantification of the intracellular DyLight 488 signal intensities in (A). One-way ANOVA with Tukey's post-hoc test. Data are represented as mean ± SEM.

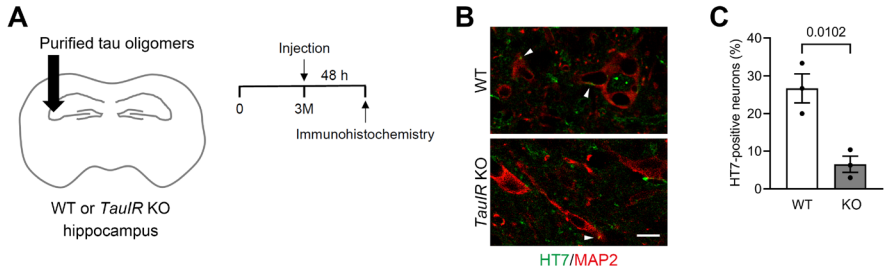

Figure 3.8. *TauIR* deficiency reduces neuronal tau uptake in mouse hippocampus.

(**A**) The hippocampal tissues of 3-month-old WT and *TauIR* KO mice were intracranially injected with purified tau oligomers (total 6 μg). (**B**) After 48 h of injection, brain sections of the hippocampus were immunostained with anti-human tau (HT7) and anti-MAP2 antibodies. Arrow heads, internalized tau oligomers. Scale bar, 10 μm. (**C**) Percentages of human tau-positive neurons in the injection area were determined. Data are represented as mean ± SEM. Unpaired *t*-test, two-tailed, $n = 3$ per group.

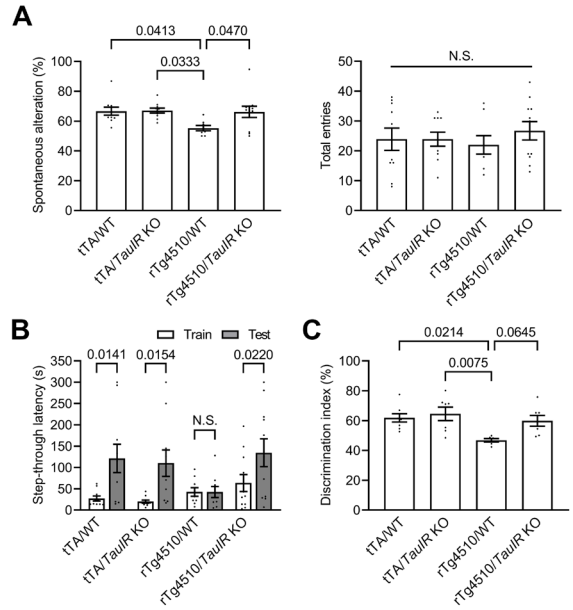

Figure 3.9. *TauIR* deficiency ameliorates cognitive impairment in rTg4510 mice.

(**A**-**C**) The 6-month-old rTA/WT, rTA/*TauIR* KO, rTg4510/WT and rTg4510/*TauIR* KO mice (four groups) were analyzed with the Y-maze test [A, two-way ANOVA with Tukey test, n = 10 (7 males and 3 females), 10 (2 males and 8 females), 8 (6 males and 2 females), 11 (4 males and 7 females) for these groups], passive avoidance test [B, paired t-test, n = 10 (7 males and 3 females), 10 (2 males and 8 females), 9 (6 males and 3 females), 11 (4 males and 7 females)] and novel object recognition test [C, two-way ANOVA with Tukey test, n = 8 (5 males and 3 females), 7 (2 males and 5 females), 6 (4 males and 2 females), 7 (4 males and 3 females)]. Data are represented as mean ± SEM.

3.3. Materials and Methods

Recombinant tau purification, fluorescence labelling and fibrillation

Human 0N4R tau was subcloned into pET-6xHis vector as previously described (Kim et al., 2016), expressed in BL21-DE3, and purified using Ni-NTA agarose (Qiagen). Tau monomer was incubated with DyLight 488 or 594 NHS Ester (Thermo Fisher Scientific) for fluorescence labelling. For tau oligomer preparation, 24 μM tau monomer was incubated with 5 mM dithiothreitol (DTT) and 6 μM heparin in PBS, and the mixture was incubated for 1 h (low-molecular-weight) or 1.5 h (high-molecular-weight) at room temperature without agitation.

Plasmid construction

Human TauIR was amplified by PCR from cDNA library and subcloned into pEGFP-N1.

Cell culture, DNA transfection and chemical treatment

HEK-Blue Null1, HEK-Blue hTauIR (InvivoGen) and BV2 cells were maintained in DMEM/high glucose medium (HyClone) containing 10% fetal bovine serum (FBS), 100 U/ml Penicillin-Streptomycin, and 10 μg/ml Gentamicin (Gibco). Cells were grown at 37°C under an atmosphere of 5% CO_2. Cells were transfected using polyethylenimine (Sigma-Aldrich) according to the manufacturer's instruction.

TauIR reporter assay

A negative control buffer, rTau or anti-TauIR antibody were treated into 96 well plate. HEK-Blue hTauIR cells (5.4×10^4 cells per well) were seeded into the 96 well plate containing reagents with a volume of 180 μl per well. After 20 h, the levels of SEAP were determined using a spectrophotometer at 620 nm.

Primary cultures of microglia and neurons

The WT and *TauIR* KO (The Jackson Laboratory) mouse primary microglia were prepared from the cortices of postnatal day 1 pups and maintained in DMEM medium containing 10% FBS, 100 U/ml Penicillin-Streptomycin, and 10 μg/ml Gentamicin. Mouse primary hippocampal neurons were prepared from embryonic day 16.5. The neurons were plated on culture plates coated with poly-L-lysine, and maintained in Neurobasal medium (Gibco) containing 2% B-27 supplement (Gibco), 100 U/ml Penicillin-Streptomycin, 10 μg/ml Gentamicin, and 1% GlutaMAX supplement (Gibco).

Tau uptake assay in primary cultured cells

Mouse primary microglia at 14 days *in vitro* (DIV 14) were incubated for 24 h with 125 nM DyLight 488-tau oligomers. Mouse primary hippocampal neurons (DIV 7) were incubated for 24 h with 50 nM DyLight 488-tau

oligomers. TauIR-mediated tau internalization was blocked by co-treatment of DyLight 488-tau oligomers and anti-TauIR antibody. Cells were washed with PBS, fixed with 4% paraformaldehyde, and processed for immunocytochemistry. Images were obtained using confocal laser scanning microscopy LSM700 (Carl Zeiss) and intracellular tau signal intensities were measured using ImageJ.

Measurement of pro-inflammatory cytokine mRNA levels by qRT-PCR

THP-1 cells were incubated at 37°C with or without 10 μg/ml recombinant tau (rTau, rPeptide) in the presence or absence of anti-TauIR antibody (100 nM and 500 nM), which was added to the culture medium simultaneously with rTau treatment. After 24 or 48 h, cells were harvested and RNA extraction was performed using the RNeasy Plus Mini Kit according to the manufacturer's instructions. The cDNA was synthesized using the QuantiTest reverse transcription kit according to the manufacturer's guidelines. The cDNA was amplified using Quantstudio 5 real-time PCR system with SYBR Green master mix.

Tau uptake in mouse hippocampus following intracranial injection

The 3-month-old mice (male) were anesthetized with a mixture of tiletamine/zolazepam (30 mg/kg) and xylazine (10 mg/kg), and intracranially injected with 6 μg of purified tau oligomers into the hippocampus (stereotaxic coordinates: anteroposterior = –2.1 mm,

mediolateral = 1.8 mm, and dorsoventral = –2.0 mm from bregma) using 30-gauge Hamilton microsyringe. After 48 h, mice were anesthetized and perfused with PBS containing 10 U/ml heparin and 4% paraformaldehyde. Brain sections (40 μm) were prepared from the hippocampus and processed for immunohistochemistry. Images were obtained using confocal laser scanning microscopy LSM700 and counted for human tau-positive cells in the injection area.

Behavioral tests

The rTg4510 mice were obtained by crossing the human P301L tau responder line (The Jackson Laboratory, #015815) to a tetracycline-controlled transactivator (tTA) line (The Jackson Laboratory, #016198). The rTg4510/*TauIR* KO mice and its control tTA/*TauIR* KO mice were obtained by crossing to *TauIR* KO mice. The 6-month-old mice (male and female) were analyzed with Y-maze, novel object recognition, and passive avoidance tests.

Y-maze test - Mice were placed in the end of one arm of Y-shaped maze (32.5 cm length x 15 cm height) and allowed to move freely for 7 min. An entry into the arm was counted when the whole body including tail is placed in the arm. The percentage of spontaneous alterations was estimated as the ratio of the number of alterations to the total number of entries.

Novel object recognition test - Mice were placed in the chamber (30 cm length x 30 cm width x 25 cm height) to move freely for 7 min at 24 h intervals. Before the test period, mice were habituated in the empty chamber for 2 days. During 3 days of test period, two objects were placed in the chamber and one of the objects were changed every day (novel object) while the other kept unchanged (familiar object). The object exploration was defined as mouse sniffing or touching the object with nose towards it. The object discrimination index was estimated as the ratio of the time of exploring a novel object to the total time of exploring objects.

Passive avoidance test - An apparatus with a light and dark compartments (20 x 20 x 20 cm each) separated by a sliding door was used for the test. Mice were placed in the closed light compartment and allowed to move freely for 1 min before opening the door. For conditioning, the latency time for the mice entering the dark compartment was measured and an electric shock (0.25 mA, 2 s) was delivered by the floor grids after closing the door. For the test, mice were placed in the closed light compartment 24 h after conditioning, allowed to move freely for 1 min before opening the door, and the latency time for the mice entering the dark compartment was measured with a 5 min cut-off.

Immunocytochemistry and immunohistochemistry

For immunocytochemistry, cells were washed with PBS and fixed with 4% paraformaldehyde for 20 min. After washing with PBS, cells were blocked

for 1 h with 3% BSA in PBS and incubated with primary antibodies in PBS containing 1% BSA overnight at 4℃. Cells were incubated for 1.5 h with Alexa Flour 488 or 594 secondary antibodies (Jackson ImmunoResearch Laboratories; 1:500). The coverslips were placed on the slides with mounting medium (Sigma-Aldrich). For immunohistochemistry, brain sections (40 μm) were prepared, washed with PBS, blocked for 1 h with 10% FBS in PBS containing 1% Triton X-100, and incubated with primary antibodies in PBS containing 5% FBS and 0.1% Triton X-100 overnight at 4℃. After washed, sections were incubated for 1.5 h with Alexa Flour 405, 488, or 594 secondary antibodies (Jackson ImmunoResearch Laboratories; 1:500). The sections were placed on the slides with mounting medium.

Statistics

All statistical analyses were performed using GraphPad Prism 9 Software. Sample sizes and the number of replicates were described in each figure legends. Normality of data distribution was assessed using the Shapiro-Wilk test and non-parametric tests were used when the data did not meet the assumptions of the parametric tests. Unpaired *t*-test or Mann-Whitney test was performed when comparing two independent groups. One-way ANOVA or two-way ANOVA test with Tukey test was performed when comparing multiple groups. Paired *t*-test was performed when analyzing passive avoidance test data. *P* values were obtained from two-tailed test. No statistical test was used to predetermine sample size.

Study approval

All mice used in this study were maintained in a specific pathogen-free animal facility. All housing, breeding, and procedures were performed according to the Korean Ministry of Food and Drug Safety (MFDS) and approved by Seoul National University Animal Care and Use Committee.

Chapter 4. Discussion

Recent studies of neurodegenerative diseases have aimed to shed light on the mechanisms underlying the propagation of protein aggregates (Vaquer-Alicea & Diamond, 2019; Peng et al., 2020). In the present study, I investigated the mechanism of tau pathogenesis, focusing on the membrane receptor through which pathological tau proteins propagate between neurons (Figure 4.1).

By establishing cell-based tau oligomer uptake assays and performing genome-wide gain-of-function screen, several membrane receptor candidates affecting tau uptake into neuronal cells were successfully isolated. A gain-of-function screen often has an advantage over a loss-of-function screen in that it enables one to isolate tau receptors in cells that lack a signal/axis for tau uptake. An important question raised by the results of our screen is why there are a number of receptors responsible for tau uptake, including HSPG, LRP1 and RAGE. In this study, RAGE contributed to cellular uptake of highly phosphorylated and AD pathology-related tau proteins present in rTg4510 mice and the CSF of AD patients. While the biochemical properties of these pathogenic tau forms are not yet clear, it is conceivable that diverse tau strains are subject to protein propagation. Consequently, assessing the uptake of diverse tau strains may reveal various strain-specific receptors of different cell types and different tauopathies. I could not find structural similarities between tau receptor candidates

isolated from the tau uptake screen. However, I found that CD47 contains Ig-like V-type domain, which is also present in RAGE and HSPG2. Notably, Ig-like V-type domain is also present in SORL1 and TREM2, which play an important role in AD pathogenesis (Rogaeva et al., 2007; Gratuze et al., 2018). It would be interesting to investigate whether proteins containing Ig-like V-type domain function in tau pathogenesis.

RAGE is known to be tightly linked to amyloid pathology (Yan et al., 2012; Cai et al., 2016). Given that RAGE expression is upregulated in various cell types in the AD brain, it may have multiple functions that contribute to the pathogenesis (Lue et al., 2001; Sasaki et al., 2001). For example, RAGE binding to Aβ induces neurotoxicity in neurons, triggers inflammatory responses in glial cells, and mediates Aβ transport across the blood-brain barrier in endothelial cells, all of which aggravate amyloid pathology in the central nervous system (Yan et al., 1996; Deane et al., 2003; Fang et al., 2010). In this study, I showed that RAGE is also linked to tau pathology by affecting transsynaptic tau propagation in neurons and inflammatory responses in microglia. Despite its lower expression in neurons than glial cells, tau-mediated induction of RAGE expression in neurons may provide a basis for its role in tau propagation. The presence of Aβ accumulation may also upregulate RAGE expression and accelerate tau pathogenesis (Pooler et al., 2015; He et al., 2018), thereby function as a pivotal receptor in AD pathogenesis. In this study, I analyzed the function of

RAGE in rTg4510 mice to rule out Aβ effect on RAGE and focus on tau pathogenesis. Since RAGE binds both Aβ and tau, it would be worth evaluating the function of RAGE in AD model mice showing both amyloid and tau pathology, such as 3xTg-AD mice.

In this study, knockout of RAGE or blocking its function ameliorates tau-induced cognitive impairment in rTg4510 mice. Although the efficacy of RAGE antagonist on tau pathogenesis has to be further validated in other mouse models to exclude other factors from genomic disruption in rTg4510 mice (Gamache et al., 2019), this study suggests a therapeutic approach that targets the process of tau propagation in AD or primary tauopathy. Previously, RAGE antagonist Azeliragon was the subject of a phase 3 clinical trial testing its ability to suppress amyloid-related pathology and inflammation in patients with AD; however, the trial was terminated with no significant relief in AD pathology. While there are several possible reasons for this failure, the clinical studies may have overlooked reductions in tau pathology due to a lack of suitable tau biomarkers. In addition, I observed that FPS-ZM1 treatment at early stages of the disease was protective of cognitive function in tauopathy model mice. It therefore may be worth evaluating efficacy of RAGE antagonists at early stages of the disease in patients with AD or primary tauopathy before there is widespread development of tau pathology. In pathologic conditions with elevated RAGE expression levels, for example in AD patients with diabetes or vascular diseases, RAGE may function as a main pathologic receptor and

therefore targeting RAGE may be an effective therapeutic strategy. Recent clinical trials on AD are targeting Aβ or tau by immunotherapy. Together with targeting the misfolded proteins, blocking their receptors may enhance the therapeutic benefit by reducing neuronal transmission and neuroinflammation.

By targeting TauIR using anti-TauIR monoclonal antibody, I could efficiently block cellular tau uptake, which leads to decreased microglial inflammatory responses and neuronal tau transmission. Similarly, recent studies have reported that immunotherapy targeting TauIR alleviates α-synuclein pathology progression in Parkinson's disease (Kim et al., 2013, 2015, 2018). Since accumulating evidence indicates there is a significant overlap in the receptor-ligand interactions among proteinopathies with different protein aggregate deposits (Chen et al., 2017; Surguchev et al., 2019; Peng et al., 2020), it would be worth evaluating the pathophysiological role of TauIR in various neurodegenerative diseases.

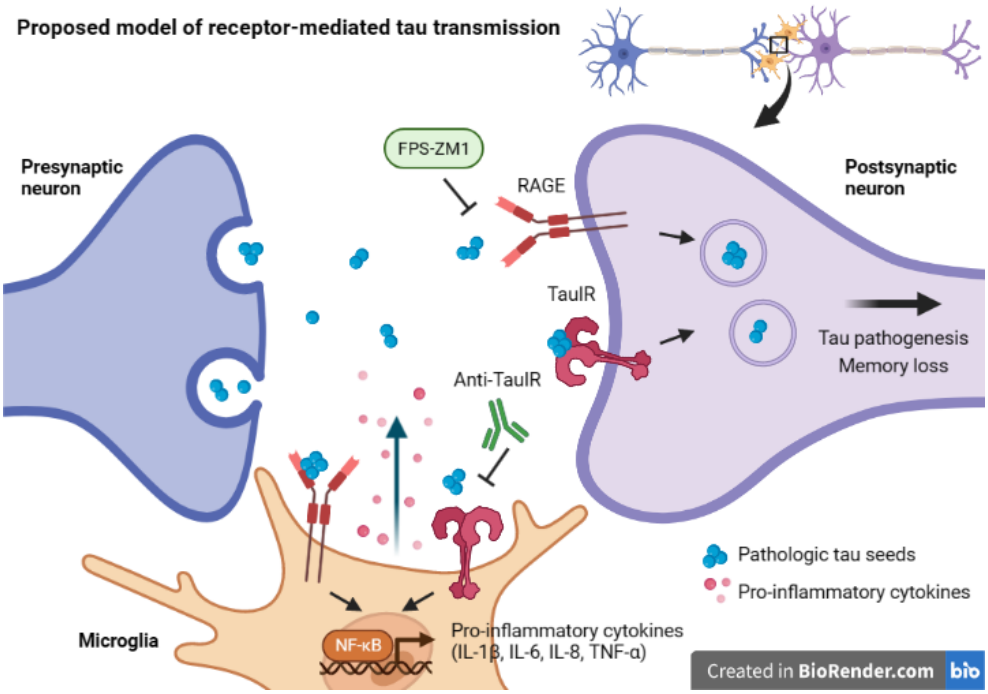

Figure 4.1. Proposed model of receptor-mediated tau transmission.

A membrane receptors RAGE and TauIR bind and internalize pathologic tau seeds into neurons and microglia. RAGE and TauIR mediate transsynaptic tau transmission in neurons, and mediate pro-inflammatory responses in microglia, which exert neurotoxic effect and promote tau pathogenesis. However, treatment of RAGE antagonist FPS-ZM1 or anti-TauIR antibody efficiently blocks the binding of tau to RAGE or TauIR, respectively, and alleviates tau pathogenesis. This model suggests that blocking the function of RAGE and TauIR may suppress the progression of tau pathology and development of memory loss in Alzheimer's disease.

References

Alquezar, C., Arya, S., & Kao, A. W. (2021). Tau Post-translational Modifications: Dynamic Transformers of Tau Function, Degradation, and Aggregation. *Frontiers in Neurology*, *11*. https://www.frontiersin.org/articles/10.3389/fneur.2020.595532

Ahmad, B., & Choi, S. (2022). Unraveling the Tomaralimab Epitope on the Toll-like Receptor 2 via Molecular Dynamics and Deep Learning. ACS Omega, 7(32), 28226–28237. https://doi.org/10.1021/acsomega.2c02559

Amos, L. A. (2004). Microtubule structure and its stabilisation. *Organic & Biomolecular Chemistry*, *2*(15), 2153–2160. https://doi.org/10.1039/B403634D

Asai, H., Ikezu, S., Tsunoda, S., Medalla, M., Luebke, J., Haydar, T., Wolozin, B., Butovsky, O., Kügler, S., & Ikezu, T. (2015). Depletion of microglia and inhibition of exosome synthesis halt tau propagation. *Nature Neuroscience*, *18*(11), 1584–1593. https://doi.org/10.1038/nn.4132

Biswas, S., & Kalil, K. (2018). The Microtubule-Associated Protein Tau Mediates the Organization of Microtubules and Their Dynamic Exploration of Actin-Rich Lamellipodia and Filopodia of Cortical Growth Cones. *Journal of Neuroscience*, *38*(2), 291–307. https://doi.org/10.1523/JNEUROSCI.2281-17.2017

Bongarzone, S., Savickas, V., Luzi, F., & Gee, A. D. (2017). Targeting the Receptor for Advanced Glycation Endproducts (RAGE): A Medicinal Chemistry Perspective. *Journal of Medicinal Chemistry*, *60*(17), 7213–7232. https://doi.org/10.1021/acs.jmedchem.7b00058

Bonham, L. W., Karch, C. M., Fan, C. C., Tan, C., Geier, E. G., Wang, Y., Wen, N., Broce, I. J., Li, Y., Barkovich, M. J., Ferrari, R., Hardy, J., Momeni, P., Höglinger, G., Müller, U., Hess, C. P., Sugrue, L. P., Dillon, W. P., Schellenberg, G. D., … Desikan, R. S. (2018). CXCR4 involvement in neurodegenerative diseases. *Translational Psychiatry*, *8*(1), Article 1. https://doi.org/10.1038/s41398-017-0049-7

Braak, H., & Braak, E. (1991). Neuropathological stageing of Alzheimer-related changes. *Acta Neuropathologica*, *82*(4), 239–259. https://doi.org/10.1007/BF00308809

Brown, J. A., Deng, J., Neuhaus, J., Sible, I. J., Sias, A. C., Lee, S. E., Kornak, J., Marx, G. A., Karydas, A. M., Spina, S., Grinberg, L. T., Coppola, G., Geschwind, D. H., Kramer, J. H., Gorno-Tempini, M. L., Miller, B. L., Rosen, H. J., & Seeley, W. W. (2019). Patient-Tailored, Connectivity-Based Forecasts of Spreading Brain Atrophy. *Neuron*, *104*(5), 856-868.e5. https://doi.org/10.1016/j.neuron.2019.08.037

Caceres, A., & Kosik, K. S. (1990). Inhibition of neurite polarity by tau antisense oligonucleotides in primary cerebellar neurons. *Nature*, *343*(6257), Article 6257. https://doi.org/10.1038/343461a0

Cai, Z., Liu, N., Wang, C., Qin, B., Zhou, Y., Xiao, M., Chang, L., Yan, L.-J., & Zhao, B. (2016). Role of RAGE in Alzheimer's Disease. *Cellular and Molecular Neurobiology*, *36*(4), 483–495. https://doi.org/10.1007/s10571-015-0233-3

Calafate, S., Flavin, W., Verstreken, P., & Moechars, D. (2016). Loss of Bin1 Promotes the Propagation of Tau Pathology. *Cell Reports*, *17*(4), 931–940. https://doi.org/10.1016/j.celrep.2016.09.063

Chen, G., Xu, T., Yan, Y., Zhou, Y., Jiang, Y., Melcher, K., & Xu, H. E. (2017). Amyloid beta: Structure, biology and structure-based therapeutic development. *Acta Pharmacologica Sinica*, *38*(9), Article 9. https://doi.org/10.1038/aps.2017.28

Chen, K., Iribarren, P., Hu, J., Chen, J., Gong, W., Cho, E. H., Lockett, S., Dunlop, N. M., & Wang, J. M. (2006). Activation of Toll-like Receptor 2 on Microglia Promotes Cell Uptake of Alzheimer Disease-associated Amyloid β Peptide*. *Journal of Biological Chemistry*, *281*(6), 3651–3659. https://doi.org/10.1074/jbc.M508125200

Clavaguera, F., Akatsu, H., Fraser, G., Crowther, R. A., Frank, S., Hench, J., Probst, A., Winkler, D. T., Reichwald, J., Staufenbiel, M., Ghetti, B., Goedert, M., & Tolnay, M. (2013). Brain homogenates from human tauopathies induce tau inclusions in mouse brain. *Proceedings of the National Academy of Sciences*, *110*(23), 9535–9540. https://doi.org/10.1073/pnas.1301175110

Clavaguera, F., Bolmont, T., Crowther, R. A., Abramowski, D., Frank, S., Probst, A., Fraser, G., Stalder, A. K., Beibel, M., Staufenbiel, M., Jucker, M., Goedert, M., & Tolnay, M. (2009). Transmission and spreading of tauopathy in transgenic mouse brain. *Nature Cell Biology*, *11*(7), 909–913. https://doi.org/10.1038/ncb1901

Daborg, J., von Otter, M., Sjölander, A., Nilsson, S., Minthon, L., Gustafson, D. R., Skoog, I., Blennow, K., & Zetterberg, H. (2010). Association of the RAGE G82S polymorphism with Alzheimer's disease. *Journal of Neural Transmission*, *117*(7), 861–867. https://doi.org/10.1007/s00702-010-0437-0

Dawson, H. N., Ferreira, A., Eyster, M. V., Ghoshal, N., Binder, L. I., & Vitek, M. P. (2001). Inhibition of neuronal maturation in primary hippocampal neurons from τ deficient mice. *Journal of Cell Science*, *114*(6), 1179–1187. https://doi.org/10.1242/jcs.114.6.1179

Deane, R., Du Yan, S., Submamaryan, R. K., LaRue, B., Jovanovic, S., Hogg, E., Welch, D., Manness, L., Lin, C., Yu, J., Zhu, H., Ghiso, J., Frangione, B., Stern, A., Schmidt, A. M., Armstrong, D. L., Arnold, B., Liliensiek, B., Nawroth, P., … Zlokovic, B. (2003). RAGE mediates amyloid-β peptide transport across the blood-brain barrier and accumulation in brain. *Nature Medicine*, *9*(7), 907–913. https://doi.org/10.1038/nm890

Deane, R., Singh, I., Sagare, A. P., Bell, R. D., Ross, N. T., LaRue, B., Love, R., Perry, S., Paquette, N., Deane, R. J., Thiyagarajan, M., Zarcone, T., Fritz, G., Friedman, A. E., Miller, B. L., & Zlokovic, B. V. (2012). A multimodal RAGE-specific inhibitor reduces amyloid β-mediated brain disorder in a mouse model of Alzheimer disease. *The Journal of Clinical Investigation*, *122*(4), 1377–1392. https://doi.org/10.1172/JCI58642

de Calignon, A., Polydoro, M., Suárez-Calvet, M., William, C., Adamowicz, D. H., Kopeikina, K. J., Pitstick, R., Sahara, N., Ashe, K. H., Carlson, G. A., Spires-Jones, T. L., & Hyman, B. T. (2012). Propagation of Tau Pathology in a Model of Early Alzheimer's Disease. *Neuron*, *73*(4), 685–697. https://doi.org/10.1016/j.neuron.2011.11.033

Dzamko, N., Gysbers, A., Perera, G., Bahar, A., Shankar, A., Gao, J., Fu, Y., & Halliday, G. M. (2017). Toll-like receptor 2 is increased in neurons in Parkinson's disease brain and may contribute to alpha-synuclein pathology. *Acta Neuropathologica*, *133*(2), 303–319. https://doi.org/10.1007/s00401-016-1648-8

Evans, L. D., Wassmer, T., Fraser, G., Smith, J., Perkinton, M., Billinton, A., & Livesey, F. J. (2018). Extracellular Monomeric and Aggregated Tau Efficiently Enter Human Neurons through Overlapping but Distinct Pathways. *Cell Reports*, *22*(13), 3612–3624. https://doi.org/10.1016/j.celrep.2018.03.021

Fang, F., Lue, L.-F., Yan, S., Xu, H., Luddy, J. S., Chen, D., Walker, D. G., Stern, D. M., Yan, S., Schmidt, A. M., Chen, J. X., & Yan, S. S. (2010). RAGE-dependent signaling in microglia contributes to neuroinflammation, Aβ accumulation, and impaired learning/memory in a mouse model of Alzheimer's disease. *The FASEB Journal*, *24*(4), 1043–1055. https://doi.org/10.1096/fj.09-139634

Fiebich, B. L., Batista, C. R. A., Saliba, S. W., Yousif, N. M., & de Oliveira, A. C. P. (2018). Role of Microglia TLRs in Neurodegeneration. *Frontiers in Cellular Neuroscience*, *12*. https://doi.org/10.3389/fncel.2018.00329

Frost, B., Jacks, R. L., & Diamond, M. I. (2009). Propagation of Tau Misfolding from the Outside to the Inside of a Cell. *Journal of Biological Chemistry*, *284*(19), 12845–12852. https://doi.org/10.1074/jbc.M808759200

Gamache, J., Benzow, K., Forster, C., Kemper, L., Hlynialuk, C., Furrow, E., Ashe, K. H., & Koob, M. D. (2019). Factors other than hTau overexpression that contribute to tauopathy-like phenotype in rTg4510 mice. *Nature Communications*, *10*(1), 2479. https://doi.org/10.1038/s41467-019-10428-1

Ghosh, S., Wu, M. D., Shaftel, S. S., Kyrkanides, S., LaFerla, F. M., Olschowka, J. A., & O'Banion, M. K. (2013). Sustained Interleukin-1β Overexpression Exacerbates Tau Pathology Despite Reduced Amyloid Burden in an Alzheimer's Mouse Model. *Journal of Neuroscience*, *33*(11), 5053–5064. https://doi.org/10.1523/JNEUROSCI.4361-12.2013

Gordon, B. A., Friedrichsen, K., Brier, M., Blazey, T., Su, Y., Christensen, J., Aldea, P., McConathy, J., Holtzman, D. M., Cairns, N. J., Morris, J. C., Fagan, A. M., Ances, B. M., & Benzinger, T. L. S. (2016). The relationship between cerebrospinal fluid markers of Alzheimer pathology and positron emission tomography tau imaging. *Brain*, *139*(8), 2249–2260. https://doi.org/10.1093/brain/aww139

Gratuze, M., Leyns, C. E. G., & Holtzman, D. M. (2018). New insights into the role of TREM2 in Alzheimer's disease. Molecular Neurodegeneration, 13(1), 66. https://doi.org/10.1186/s13024-018-0298-9

Guo, J. L., Narasimhan, S., Changolkar, L., He, Z., Stieber, A., Zhang, B., Gathagan, R. J., Iba, M., McBride, J. D., Trojanowski, J. Q., & Lee, V. M. Y. (2016). Unique pathological tau conformers from Alzheimer's brains transmit tau pathology in nontransgenic mice. *Journal of Experimental Medicine*, *213*(12), 2635–2654. https://doi.org/10.1084/jem.20160833

He, Z., Guo, J. L., McBride, J. D., Narasimhan, S., Kim, H., Changolkar, L., Zhang, B., Gathagan, R. J., Yue, C., Dengler, C., Stieber, A., Nitla, M., Coulter, D. A., Abel, T., Brunden, K. R., Trojanowski, J. Q., & Lee, V. M.-Y. (2018). Amyloid-β plaques enhance Alzheimer's brain tau-seeded pathologies by facilitating neuritic plaque tau aggregation. *Nature Medicine*, *24*(1), Article 1. https://doi.org/10.1038/nm.4443

Hofmann, M. A., Drury, S., Hudson, B. I., Gleason, M. R., Qu, W., Lu, Y., Lalla, E., Chitnis, S., Monteiro, J., Stickland, M. H., Bucciarelli, L. G., Moser, B., Moxley, G., Itescu, S., Grant, P. J., Gregersen, P. K., Stern, D. M., & Schmidt, A. M. (2002). RAGE and arthritis: The G82S polymorphism amplifies the inflammatory response. *Genes & Immunity*, *3*(3), Article 3. https://doi.org/10.1038/sj.gene.6363861

Holmes, B. B., DeVos, S. L., Kfoury, N., Li, M., Jacks, R., Yanamandra, K., Ouidja, M. O., Brodsky, F. M., Marasa, J., Bagchi, D. P., Kotzbauer, P. T., Miller, T. M., Papy-Garcia, D., & Diamond, M. I. (2013). Heparan sulfate proteoglycans mediate internalization and propagation of specific proteopathic seeds. *Proceedings of the National Academy of Sciences*, *110*(33), E3138–E3147. https://doi.org/10.1073/pnas.1301440110

Javanmehr, N., Saleki, K., Alijanizadeh, P., & Rezaei, N. (2022). Microglia dynamics in aging-related neurobehavioral and neuroinflammatory diseases. *Journal of Neuroinflammation*, *19*(1), 273. https://doi.org/10.1186/s12974-022-02637-1

Jonsson, T., Stefansson, H., Steinberg, S., Jonsdottir, I., Jonsson, P. V., Snaedal, J., Bjornsson, S., Huttenlocher, J., Levey, A. I., Lah, J. J., Rujescu, D., Hampel, H., Giegling, I., Andreassen, O. A., Engedal, K., Ulstein, I., Djurovic, S., Ibrahim-Verbaas, C., Hofman, A., … Stefansson, K. (2013). Variant of TREM2 Associated with the Risk of Alzheimer's Disease. *New England Journal of Medicine*, *368*(2), 107–116. https://doi.org/10.1056/NEJMoa1211103

Kam, T.-I., Song, S., Gwon, Y., Park, H., Yan, J.-J., Im, I., Choi, J.-W., Choi, T.-Y., Kim, J., Song, D.-K., Takai, T., Kim, Y.-C., Kim, K.-S., Choi, S.-Y., Choi, S., Klein, W. L., Yuan, J., & Jung, Y.-K. (2013). FcγRIIb mediates amyloid-β neurotoxicity and memory impairment in Alzheimer's disease. *The Journal of Clinical Investigation*, *123*(7), 2791–2802. https://doi.org/10.1172/JCI66827

Kaufman, S. K., Sanders, D. W., Thomas, T. L., Ruchinskas, A. J., Vaquer-Alicea, J., Sharma, A. M., Miller, T. M., & Diamond, M. I. (2016). Tau Prion Strains Dictate Patterns of Cell Pathology, Progression Rate, and Regional Vulnerability In Vivo. *Neuron*, *92*(4), 796–812. https://doi.org/10.1016/j.neuron.2016.09.055

Kidd, M. (1963). Paired Helical Filaments in Electron Microscopy of Alzheimer's Disease. *Nature*, *197*(4863), Article 4863. https://doi.org/10.1038/197192b0

Kierdorf, K., & Fritz, G. (2013). RAGE regulation and signaling in inflammation and beyond. *Journal of Leukocyte Biology*, *94*(1), 55–68. https://doi.org/10.1189/jlb.1012519

Kim, C., Ho, D.-H., Suk, J.-E., You, S., Michael, S., Kang, J., Joong Lee, S., Masliah, E., Hwang, D., Lee, H.-J., & Lee, S.-J. (2013). Neuron-released oligomeric α-synuclein is an endogenous agonist of TLR2 for paracrine activation of microglia. *Nature Communications*, *4*(1), 1562. https://doi.org/10.1038/ncomms2534

Kim, C., Rockenstein, E., Spencer, B., Kim, H.-K., Adame, A., Trejo, M., Stafa, K., Lee, H.-J., Lee, S.-J., & Masliah, E. (2015). Antagonizing Neuronal Toll-like Receptor 2 Prevents Synucleinopathy by Activating Autophagy. *Cell Reports*, *13*(4), 771–782. https://doi.org/10.1016/j.celrep.2015.09.044

Kim, C., Spencer, B., Rockenstein, E., Yamakado, H., Mante, M., Adame, A., Fields, J. A., Masliah, D., Iba, M., Lee, H.-J., Rissman, R. A., Lee, S.-J., & Masliah, E. (2018). Immunotherapy targeting toll-like receptor 2 alleviates neurodegeneration in models of synucleinopathy by modulating α-synuclein transmission and neuroinflammation. *Molecular Neurodegeneration*, *13*(1), 43. https://doi.org/10.1186/s13024-018-0276-2

Kim, Y., Choi, H., Lee, W., Park, H., Kam, T.-I., Hong, S., Nah, J., Jung, S., Shin, B., Lee, H., Choi, T.-Y., Choo, H., Kim, K.-K., Choi, S.-Y., Kayed, R., & Jung, Y.-K. (2016). Caspase-cleaved tau exhibits rapid memory impairment associated with tau oligomers in a transgenic mouse model. *Neurobiology of Disease*, *87*, 19–28. https://doi.org/10.1016/j.nbd.2015.12.006

Kinney, J. W., Bemiller, S. M., Murtishaw, A. S., Leisgang, A. M., Salazar, A. M., & Lamb, B. T. (2018). Inflammation as a central mechanism in Alzheimer's disease. *Alzheimer's & Dementia: Translational Research & Clinical Interventions*, *4*(1), 575–590. https://doi.org/10.1016/j.trci.2018.06.014

Knowles, T. P. J., Vendruscolo, M., & Dobson, C. M. (2014). The amyloid state and its association with protein misfolding diseases. *Nature Reviews Molecular Cell Biology*, *15*(6), Article 6. https://doi.org/10.1038/nrm3810

Lambert, J.-C., Ibrahim-Verbaas, C. A., Harold, D., Naj, A. C., Sims, R., Bellenguez, C., Jun, G., DeStefano, A. L., Bis, J. C., Beecham, G. W., Grenier-Boley, B., Russo, G., Thornton-Wells, T. A., Jones, N., Smith, A. V., Chouraki, V., Thomas, C., Ikram, M. A., Zelenika, D., … Amouyel, P. (2013). Meta-analysis of 74,046 individuals identifies 11 new susceptibility loci for Alzheimer's disease. *Nature Genetics*, *45*(12), Article 12. https://doi.org/10.1038/ng.2802

Lasagna-Reeves, C. A., Castillo-Carranza, D. L., Sengupta, U., Guerrero-Munoz, M. J., Kiritoshi, T., Neugebauer, V., Jackson, G. R., & Kayed, R. (2012). Alzheimer brain-derived tau oligomers propagate pathology from endogenous tau. Scientific Reports, 2(1), Article 1. https://doi.org/10.1038/srep00700

Lee, G., Cowan, N., & Kirschner, M. (1988). The Primary Structure and Heterogeneity of Tau Protein from Mouse Brain. *Science*, *239*(4837), 285–288. https://doi.org/10.1126/science.3122323

Li, K., Dai, D., Zhao, B., Yao, L., Yao, S., Wang, B., & Yang, Z. (2009). Association between the RAGE G82S polymorphism and Alzheimer's disease. *Journal of Neural Transmission*, *117*(1), 97. https://doi.org/10.1007/s00702-009-0334-6

Lue, L.-F., Walker, D. G., Brachova, L., Beach, T. G., Rogers, J., Schmidt, A. M., Stern, D. M., & Yan, S. D. (2001). Involvement of Microglial Receptor for Advanced Glycation Endproducts (RAGE) in Alzheimer's Disease: Identification of a Cellular Activation Mechanism. *Experimental Neurology*, *171*(1), 29–45. https://doi.org/10.1006/exnr.2001.7732

Mirbaha, H., Chen, D., Morazova, O. A., Ruff, K. M., Sharma, A. M., Liu, X., Goodarzi, M., Pappu, R. V., Colby, D. W., Mirzaei, H., Joachimiak, L. A., & Diamond, M. I. (2018). Inert and seed-competent tau monomers suggest structural origins of aggregation. *ELife*, *7*, e36584. https://doi.org/10.7554/eLife.36584

Momtazmanesh, S., Perry, G., & Rezaei, N. (2020). Toll-like receptors in Alzheimer's disease. *Journal of Neuroimmunology*, *348*, 577362. https://doi.org/10.1016/j.jneuroim.2020.577362

Osawa, M., Yamamoto, Y., Munesue, S., Murakami, N., Sakurai, S., Watanabe, T., Yonekura, H., Uchigata, Y., Iwamoto, Y., & Yamamoto, H. (2007). De-N-glycosylation or G82S mutation of RAGE sensitizes its interaction with advanced glycation endproducts. *Biochimica et Biophysica Acta (BBA) - General Subjects*, *1770*(10), 1468–1474. https://doi.org/10.1016/j.bbagen.2007.07.003

Paolicelli, R. C., Sierra, A., Stevens, B., Tremblay, M.-E., Aguzzi, A., Ajami, B., Amit, I., Audinat, E., Bechmann, I., Bennett, M., Bennett, F., Bessis, A., Biber, K., Bilbo, S., Blurton-Jones, M., Boddeke, E., Brites, D., Brône, B., Brown, G. C., … Wyss-Coray, T. (2022). Microglia states and nomenclature: A field at its crossroads. *Neuron*, *110*(21), 3458–3483. https://doi.org/10.1016/j.neuron.2022.10.020

Park, H., Kam, T.-I., Kim, Y., Choi, H., Gwon, Y., Kim, C., Koh, J.-Y., & Jung, Y.-K. (2012). Neuropathogenic role of adenylate kinase-1 in Aβ-mediated tau phosphorylation via AMPK and GSK3β. *Human Molecular Genetics*, *21*(12), 2725–2737. https://doi.org/10.1093/hmg/dds100

Park, J. W., Vahidi, B., Taylor, A. M., Rhee, S. W., & Jeon, N. L. (2006). Microfluidic culture platform for neuroscience research. *Nature Protocols*, *1*(4), 2128–2136. https://doi.org/10.1038/nprot.2006.316

Park, S. J., Kleffmann, T., & Hessian, P. A. (2011). The G82S Polymorphism Promotes Glycosylation of the Receptor for Advanced Glycation End Products (RAGE) at Asparagine 81 COMPARISON OF WILD-TYPE RAGE WITH THE G82S POLYMORPHIC VARIANT. *Journal of Biological Chemistry*, *286*(24), 21384–21392. https://doi.org/10.1074/jbc.M111.241281

Peng, C., Trojanowski, J. Q., & Lee, V. M.-Y. (2020). Protein transmission in neurodegenerative disease. *Nature Reviews Neurology*, *16*(4), Article 4. https://doi.org/10.1038/s41582-020-0333-7

Pooler, A. M., Polydoro, M., Maury, E. A., Nicholls, S. B., Reddy, S. M., Wegmann, S., William, C., Saqran, L., Cagsal-Getkin, O., Pitstick, R., Beier, D. R., Carlson, G. A., Spires-Jones, T. L., & Hyman, B. T. (2015). Amyloid accelerates tau propagation and toxicity in a model of early Alzheimer's disease. *Acta Neuropathologica Communications*, *3*(1), 14. https://doi.org/10.1186/s40478-015-0199-x

Ramsden, M., Kotilinek, L., Forster, C., Paulson, J., McGowan, E., SantaCruz, K., Guimaraes, A., Yue, M., Lewis, J., Carlson, G., Hutton, M., & Ashe, K. H. (2005). Age-Dependent Neurofibrillary Tangle Formation, Neuron Loss, and Memory Impairment in a Mouse Model of Human Tauopathy (P301L). *Journal of Neuroscience*, *25*(46), 10637–10647. https://doi.org/10.1523/JNEUROSCI.3279-05.2005

Rathore, N., Ramani, S. R., Pantua, H., Payandeh, J., Bhangale, T., Wuster, A., Kapoor, M., Sun, Y., Kapadia, S. B., Gonzalez, L., Zarrin, A. A., Goate, A., Hansen, D. V., Behrens, T. W., & Graham, R. R. (2018). Paired Immunoglobulin-like Type 2 Receptor Alpha G78R variant alters ligand binding and confers protection to Alzheimer's disease. *PLOS Genetics*, *14*(11), e1007427. https://doi.org/10.1371/journal.pgen.1007427

Rauch, J. N., Luna, G., Guzman, E., Audouard, M., Challis, C., Sibih, Y. E., Leshuk, C., Hernandez, I., Wegmann, S., Hyman, B. T., Gradinaru, V., Kampmann, M., & Kosik, K. S. (2020). LRP1 is a master regulator of tau uptake and spread. *Nature*, *580*(7803), Article 7803. https://doi.org/10.1038/s41586-020-2156-5

Reed-Geaghan, E. G., Savage, J. C., Hise, A. G., & Landreth, G. E. (2009). CD14 and Toll-Like Receptors 2 and 4 Are Required for Fibrillar Aβ-Stimulated Microglial Activation. *Journal of Neuroscience*, *29*(38), 11982–11992. https://doi.org/10.1523/JNEUROSCI.3158-09.2009

Rogaeva, E., Meng, Y., Lee, J. H., Gu, Y., Kawarai, T., Zou, F., Katayama, T., Baldwin, C. T., Cheng, R., Hasegawa, H., Chen, F., Shibata, N., Lunetta, K. L., Pardossi-Piquard, R., Bohm, C., Wakutani, Y., Cupples, L. A., Cuenco, K. T., Green, R. C., … St George-Hyslop, P. (2007). The neuronal sortilin-related receptor SORL1 is genetically associated with Alzheimer disease. Nature Genetics, 39(2), 168–177. https://doi.org/10.1038/ng1943

Sanjana, N. E., Shalem, O., & Zhang, F. (2014). Improved vectors and genome-wide libraries for CRISPR screening. *Nature Methods*, *11*(8), Article 8. https://doi.org/10.1038/nmeth.3047

SantaCruz, K., Lewis, J., Spires, T., Paulson, J., Kotilinek, L., Ingelsson, M., Guimaraes, A., DeTure, M., Ramsden, M., McGowan, E., Forster, C., Yue, M., Orne, J., Janus, C., Mariash, A., Kuskowski, M., Hyman, B., Hutton, M., & Ashe, K. H. (2005). Tau Suppression in a Neurodegenerative Mouse Model Improves Memory Function. *Science*, *309*(5733), 476–481. https://doi.org/10.1126/science.1113694

Sasaki, N., Toki, S., Chowei, H., Saito, T., Nakano, N., Hayashi, Y., Takeuchi, M., & Makita, Z. (2001). Immunohistochemical distribution of the receptor for advanced glycation end products in neurons and astrocytes in Alzheimer's disease. *Brain Research*, *888*(2), 256–262. https://doi.org/10.1016/S0006-8993(00)03075-4

Schoonenboom, N. S. M., Reesink, F. E., Verwey, N. A., Kester, M. I., Teunissen, C. E., Ven, P. M. van de, Pijnenburg, Y. a. L., Blankenstein, M. A., Rozemuller, A. J., Scheltens, P., & Flier, W. M. van der. (2012). Cerebrospinal fluid markers for differential dementia diagnosis in a large memory clinic cohort. *Neurology*, *78*(1), 47–54. https://doi.org/10.1212/WNL.0b013e31823ed0f0

Sengupta, U., Portelius, E., Hansson, O., Farmer, K., Castillo-Carranza, D., Woltjer, R., Zetterberg, H., Galasko, D., Blennow, K., & Kayed, R. (2017). Tau oligomers in cerebrospinal fluid in Alzheimer's disease. *Annals of Clinical and Translational Neurology*, *4*(4), 226–235. https://doi.org/10.1002/acn3.382

Spillantini, M. G., & Goedert, M. (2013). Tau pathology and neurodegeneration. *The Lancet Neurology*, *12*(6), 609–622. https://doi.org/10.1016/S1474-4422(13)70090-5

Stelzmann, R. A., Norman Schnitzlein, H., & Reed Murtagh, F. (1995). An english translation of alzheimer's 1907 paper, "über eine eigenartige erkankung der hirnrinde." *Clinical Anatomy*, *8*(6), 429–431. https://doi.org/10.1002/ca.980080612

Surguchev, A. A., Emamzadeh, F. N., & Surguchov, A. (2019). Cell Responses to Extracellular α-Synuclein. *Molecules*, *24*(2). https://doi.org/10.3390/molecules24020305

Takeda, S., Wegmann, S., Cho, H., DeVos, S. L., Commins, C., Roe, A. D., Nicholls, S. B., Carlson, G. A., Pitstick, R., Nobuhara, C. K., Costantino, I., Frosch, M. P., Müller, D. J., Irimia, D., & Hyman, B. T. (2015). Neuronal uptake and propagation of a rare phosphorylated high-molecular-weight tau derived from Alzheimer's disease brain. *Nature Communications*, *6*, 8490. https://doi.org/10.1038/ncomms9490

Tang, S.-C., Arumugam, T. V., Xu, X., Cheng, A., Mughal, M. R., Jo, D. G., Lathia, J. D., Siler, D. A., Chigurupati, S., Ouyang, X., Magnus, T., Camandola, S., & Mattson, M. P. (2007). Pivotal role for neuronal Toll-like receptors in ischemic brain injury and functional deficits. *Proceedings of the National Academy of Sciences*, *104*(34), 13798–13803. https://doi.org/10.1073/pnas.0702553104

Vaquer-Alicea, J., & Diamond, M. I. (2019). Propagation of Protein Aggregation in Neurodegenerative Diseases. *Annual Review of Biochemistry*, *88*(1), 785–810. https://doi.org/10.1146/annurev-biochem-061516-045049

Vogel, J. W., Young, A. L., Oxtoby, N. P., Smith, R., Ossenkoppele, R., Strandberg, O. T., La Joie, R., Aksman, L. M., Grothe, M. J., Iturria-Medina, Y., Pontecorvo, M. J., Devous, M. D., Rabinovici, G. D., Alexander, D. C., Lyoo, C. H., Evans, A. C., & Hansson, O. (2021). Four distinct trajectories of tau deposition identified in Alzheimer's disease. *Nature Medicine*, *27*(5), 871–881. https://doi.org/10.1038/s41591-021-01309-6

Wang, C., Fan, L., Khawaja, R. R., Liu, B., Zhan, L., Kodama, L., Chin, M., Li, Y., Le, D., Zhou, Y., Condello, C., Grinberg, L. T., Seeley, W. W., Miller, B. L., Mok, S.-A., Gestwicki, J. E., Cuervo, A. M., Luo, W., & Gan, L. (2022). Microglial NF-κB drives tau spreading and toxicity in a mouse model of tauopathy. *Nature Communications*, *13*(1), Article 1. https://doi.org/10.1038/s41467-022-29552-6

Wang, S., & Colonna, M. (2019). Microglia in Alzheimer's disease: A target for immunotherapy. *Journal of Leukocyte Biology*, *106*(1), 219–227. https://doi.org/10.1002/JLB.MR0818-319R

Wegmann, S., Maury, E. A., Kirk, M. J., Saqran, L., Roe, A., DeVos, S. L., Nicholls, S., Fan, Z., Takeda, S., Cagsal-Getkin, O., William, C. M., Spires-Jones, T. L., Pitstick, R., Carlson, G. A., Pooler, A. M., & Hyman, B. T. (2015). Removing endogenous tau does not prevent tau propagation yet reduces its neurotoxicity. *The EMBO Journal*, *34*(24), 3028–3041. https://doi.org/10.15252/embj.201592748

Weingarten, M. D., Lockwood, A. H., Hwo, S. Y., & Kirschner, M. W. (1975). A protein factor essential for microtubule assembly. *Proceedings of the National Academy of Sciences*, *72*(5), 1858–1862. https://doi.org/10.1073/pnas.72.5.1858

Wu, J. W., Herman, M., Liu, L., Simoes, S., Acker, C. M., Figueroa, H., Steinberg, J. I., Margittai, M., Kayed, R., Zurzolo, C., Paolo, G. D., & Duff, K. E. (2013). Small Misfolded Tau Species Are Internalized via Bulk Endocytosis and Anterogradely and Retrogradely Transported in Neurons. *Journal of Biological Chemistry*, *288*(3), 1856–1870. https://doi.org/10.1074/jbc.M112.394528

Yan, S. D., Chen, X., Fu, J., Chen, M., Zhu, H., Roher, A., Slattery, T., Zhao, L., Nagashima, M., Morser, J., Migheli, A., Nawroth, P., Stern, D., & Schmidt, A. M. (1996). RAGE and amyloid-β peptide neurotoxicity in Alzheimer's disease. *Nature*, *382*(6593), Article 6593. https://doi.org/10.1038/382685a0

Yan, S. S., Chen, D., Yan, S., Guo, L., Du, H., & Chen, J. X. (2012). RAGE is a key cellular target for Abeta-induced perturbation in Alzheimer's disease. *Frontiers in Bioscience (Scholar Edition)*, *4*, 240–250. https://doi.org/10.2741/265

Yoshiyama, Y., Higuchi, M., Zhang, B., Huang, S.-M., Iwata, N., Saido, T. C., Maeda, J., Suhara, T., Trojanowski, J. Q., & Lee, V. M.-Y. (2007). Synapse Loss and Microglial Activation Precede Tangles in a P301S Tauopathy Mouse Model. *Neuron*, *53*(3), 337–351. https://doi.org/10.1016/j.neuron.2007.01.010

국문 초록

타우 병증에서 타우 응집체가 발견되는 뇌의 영역은 임상에서 나타나는 증상과 밀접하게 연관되어 있다. 비정상적인 구조를 형성한 타우 단백질은 신경 세포의 연결망을 따라 뇌의 다른 부위로 퍼져나가며, 이것이 질병의 진행을 유발한다. 이러한 타우 단백질의 전파에 대한 병리적 이해는 매우 중요하지만, 타우 단백질이 어떠한 기전을 통해 신경 세포 내로 이동하는지에 관해서는 아직 명확하게 밝혀져 있지 않다.

타우 중합체의 신경 세포 간 전파에 관여하는 세포막 수용체를 발굴하기 위해 나는 세포 기반 타우 흡수 분석법을 확립하고 cDNA 발현 라이브러리를 이용하여 스크리닝을 진행했다. 유전체 수준의 세포 기반 기능 스크리닝을 진행한 결과, 타우 중합체의 세포 흡수를 촉진하는 세포막 수용체로 RAGE (receptor for advanced glycation end products)가 동정되었다. RAGE의 결핍은 rTg4510 마우스 뇌로부터 추출한 병리적 형태의 타우 또는 알츠하이머병 환자의 뇌척수액으로부터 얻은 병리적 형태의 타우가 신경 세포 내로 흡수되는 것을 감소시켰으며, 세 개의 챔버로 분리된 미세유체 칩 상에 배양된 신경 세포 간 타우 전파를 감소시켰다. RAGE 발현 양은 rTg4510 마우스 뇌와 타우 응집체를 처리한 신경 세포에서 증가했다. RAGE가 녹아웃 된 마우스는 GFP-P301L 타우 아데노수반바이러스의 주입 후 발생하는 기억력

감퇴가 개선되었다. RAGE 길항제 FPS-ZM1를 처치한 rTg4510 마우스는 신경 세포 간 타우 전파와 염증 반응이 차단되어 인지기능 장애가 개선되었다.

또한, 나는 타우 중합체의 신경 세포 간 전파에서의 TauIR (tau immunoreceptor)의 역할을 탐구하였다. 타우는 TauIR의 활성화를 유발했고 그것은 세포 내로의 타우 흡수를 증가시켰다. TauIR의 결핍 또는 항-TauIR 항체를 이용한 TauIR의 차단은 미세아교세포로의 타우 흡수를 감소시켰다. 타우로 인한 TauIR 활성화는 전염증성 사이토카인을 증가시켰다. 신경 세포에서도 TauIR의 결핍 또는 항-TauIR 항체를 이용한 TauIR의 차단은 세포 내로의 타우 흡수를 감소시켰다. TauIR 녹아웃은 rTg4510 마우스에서 발생하는 인지기능 장애를 개선하였다.

이러한 결과들은 신경 세포와 미세아교세포에 존재하는 RAGE와 TauIR이 병리적인 타우와 결합하고 신경 세포 간 타우의 전파와 미세아교세포의 염증 반응을 촉진시킴을 시사한다. 따라서, 타우병증에서 RAGE와 TauIR의 기능을 차단하는 것은 타우 병리의 진행과 행동 결함의 발달을 저해할 수 있을 것이다.

주요어 : Tau propagation, Tau oligomer, Neuroinflammation, RAGE, Tau immunoreceptor, FPS-ZM1

학번 : 2015-20501